Received: 30 April 2020 | Revised: 21 September 2020 | Accepted: 23 September 2020

DOI: 10.1002/jcp.30113

ORIGINAL RESEARCH ARTICLE

Journal of Cellular Physiology WILEY

Cancer-associated mutations in the condensin II subunit CAPH2 cause genomic instability through telomere dysfunction and anaphase chromosome bridges

Emily Weyburne | Giovanni Bosco

Department of Molecular and Systems Biology, Dartmouth College, Hanover, New Hampshire, USA

Correspondence
Giovanni Bosco, Department of Molecular and Systems Biology, Dartmouth College, Hanover, NH 03765, USA.
Email: Giovanni.Bosco@dartmouth.edu

Funding information
Audrey and Theodor Geisel School of Medicine at Dartmouth

Abstract

Genome instability in cancer drives tumor heterogeneity, undermines the success of therapies, and leads to metastasis and recurrence. Condensins are conserved chromatin-binding proteins that promote genomic stability, mainly by ensuring proper condensation of chromatin and mitotic chromosome segregation. Condensin mutations are found in human tumors, but it is not known how or even if such mutations promote cancer progression. In this study, we focus on condensin II subunit CAPH2 and specific CAPH2 mutations reported to be enriched in human cancer patients, and we test how CAPH2 cancer-specific mutations may lead to condensin II complex dysfunction and contribute to genome instability. We find that R551P, R551S, and S556F mutations in CAPH2 cause genomic instability by causing DNA damage, anaphase defects, micronuclei, and chromosomal instability. DNA damage and anaphase defects are caused primarily by ataxia telangiectasia and Rad3-related-dependent telomere dysfunction, as anaphase bridges are enriched for telomeric repeat sequences. We also show that these mutations decrease the binding of CAPH2 to the ATPase subunit SMC4 as well as the rest of the condensin II complex, and decrease the amount of CAPH2 protein bound to chromatin. Thus, in vivo the R551P, R551S, and S556F cancer-specific CAPH2 mutant proteins are likely to impair condensin II complex formation, impede condensin II activity during mitosis and interphase, and promote genetic heterogeneity in cell populations that can lead to clonal outgrowth of cancer cells with highly diverse genotypes.

KEYWORDS
anaphase bridge, condensin, DNA damage, genome instability, telomere

[The order of the figures was updated on December 11, 2020, after online publication of this article]

1 | INTRODUCTION

The maintenance of genome integrity is essential to preserve normal gene dosage and the subsequent gene regulation necessary for the proper development and maintenance of tissues. Mutations, copy number variations, chromosomal rearrangements, and aneuploidy, individually and in combination, can contribute to inappropriate gene expression. Not surprisingly, genome instability is considered to be a defining characteristic of cancer cells (Hanahan & Weinberg, 2011), and the acquired genome instability of a cancer cell is thought to drive chromosome rearrangements and mutations that generate genetic heterogeneity within a tumor (Bakhoum & Landau, 2017; Burrell, McGranahan, et al., 2013). Because genome instability of a tumor can generate a vast amount of genetic heterogeneity in a short time period, in some cells genetic conditions are created in which cancer therapies are rendered ineffective by drug resistance, and these cells selectively proliferate and contribute to cancer progression. Although there are multiple mechanisms through which genomes can become unstable, DNA damage and errors in chromosome segregation during mitosis are two primary causes of genome instability that lead to mutations, aneuploidy, and/or structural chromosomal aberrations affecting the expression and function of large numbers of genes (Burrell, McClelland, et al., 2013; Janssen et al., 2011; Tubbs & Nussenzweig, 2017).

Condensin complexes, formed by structural maintenance of chromosomes (SMC) proteins along with their binding partners chromosome-associated proteins (CAP), are unique chromatin factors in that they play essential functions throughout the cell cycle (Hirano, 2016). Two types of condensin complexes have been studied extensively in human cells, condensin I and condensin II. Condensin I and condensin II are each composed of five subunits in a ring-like shape that encircles DNA (Kschonsak et al., 2017; Onn et al., 2007; Piazza et al., 2014). Both condensin I and condensin II complexes contain the ATPases SMC2 and SMC4, while condensin I contain the non-SMC subunits CAPD2, CAPG, and CAPH, and condensin II contains CAPD3, CAPG2, and CAPH2. In mitosis, the combined activity of condensin I and condensin II is essential for chromosome condensation (Aalbers et al., 2012; Gibcus et al., 2018; Hirano, 2016; Manning et al., 2010; Ono et al., 2004, 2003) and centromere structure (Manning et al., 2010), while only condensin II remains in the nucleus during interphase (Hirano, 2016). Interphase condensin activities modulate a three-dimensional genome organization and affect replication and transcription (Bauer et al., 2012; Coschi et al., 2014; Dowen et al., 2013; Sutani et al., 2015). Given these critical functions, it is not unexpected that condensin complexes are necessary to maintain genomic stability. One way that condensins have been linked to genomic instability is through the breakage–fusion–bridge (BFB) cycle, which causes both DNA damage and mitotic defects. The BFB cycle, first described by Barbara McClintock (McClintock, 1939, 1941), is triggered by chromosome breaks or dysfunctional telomeres that fuse into dicentric chromosomes or sister chromatids that then form anaphase chromatin bridges that eventually break and fuse again, thus the BFB cycle repeats itself. The depletion of human condensins in cultured cells is sufficient to trigger BFB cycles and large-scale genome rearrangements (Umbreit et al., 2020), consistent with previous observations that condensin mutant cells fail to resolve chromosome catenations leading to anaphase bridges (Hartl et al., 2008). The primary mechanism by which condensins normally prevent anaphase bridges remains an open question.

Our previous observations in human cells have indicated that one way that condensin II depletion may cause genome instability is by causing DNA damage throughout the genome and by triggering telomere dysfunction (Wallace et al., 2019). Telomeres of human chromosomes are tracts of TTAGGG DNA repeats found at chromosome ends (Moyzis et al., 1988). G-rich repeat sequence-specific DNA binding proteins and their accessory proteins, in combination with telomere DNA loop structures (T-loops), function to protect the chromosome end from being recognized by exonucleases and DNA damage repair enzymes (de Lange, 2018). Telomere dysfunction has been shown to cause genomic instability by generating chromosome end-to-end fusions that break and generate complex unbalanced genome rearrangements (Fouladi et al., 2000; Lo et al., 2002; McClintock, 1941; Sabatier et al., 2005). We have previously shown that CAPH2 localizes to human telomeres and binds to the shelterin subunit TRF1, while knockdown of CAPH2 causes DNA damage foci at telomeres in interphase and fragile telomere phenotypes in mitosis (Wallace et al., 2019). Fragile telomeres, like other genomic fragile sites, can be caused by DNA replication defects, or drug-induced replication stress (Durkin & Glover, 2007; Sfeir et al., 2009; Vannier et al., 2012).

Computational analysis of The Cancer Genome Atlas sequencing data for mutated pathways and complexes identified the condensin complexes as being significantly mutated in multiple cancer types, with 4.2% of samples analyzed exhibiting condensin mutations (Leiserson et al., 2015). Interestingly, the majority of the mutations were missense mutations, implying that expression of the full-length protein was maintained but the function was altered. It was not determined whether these mutations were homozygous or heterozygous (Leiserson et al., 2015). A cluster of missense mutations was found in CAPH2 between Arg551 and Ser556. To our knowledge, these or any other specific human cancer-associated CAPH2 mutations have not been functionally validated. The mechanistic basis through which cancer-associated condensin mutations may initiate or promote tumor cell proliferation is therefore not known. Since our previous observations indicated that condensin II depletion led to general DNA damage and fragile telomeres, we speculated that cancer-associated condensin II mutations may contribute to the initiation or progression of cancer by causing genome instability, possibly by triggering telomere dysfunction and end-to-end fusions.

In this present study, we aim to characterize human cancer-associated mutations in the condensin II complex, specifically in the CAPH2 protein subunit (encoded by the NCAPH2 gene in humans). We chose to characterize the mutations between Arg551 and

Ser556 of CAPH2 because the significant clustering implies that this region is important for condensin II regulation. We show that the R551P, R551S, and S556F mutations in CAPH2 impede condensin complex formation, and cause increased anaphase chromosome bridges, micronuclei, DNA damage, and chromosomal instability (CIN), at least in part through telomere dysfunction. From these data, we infer that R551P, R551S, and S556F CAPH2 mutations cause genomic instability, even in cells that retain wild-type (WT) CAPH2 expression, and suggest that these specific mutations may contribute to cancer cell genetic heterogeneity.

2 | METHODS

Protein sequence alignment

Protein sequences were aligned with the online tool PROMALS3D (Pei et al., 2008; http://prodata.swmed.edu/promals3d/promals3d.php) using the default parameters.

2.1 | Cell culture

Retinal pigment epithelial 1 (RPE1) cells were cultured in Dulbecco's modified Eagle's medium with 10% fetal bovine serum (FBS) and 1X penicillin/streptomycin (Corning) at 37°C and 5% CO_2. HCT116 cells were cultured in McCoy's 5A modified medium (Sigma) with 10% FBS and 1X penicillin/streptomycin (Corning) at 37°C and 5% CO_2. RPE1 and HCT116 cells were validated at the Vermont Cancer Center DNA Analysis Facility by STR DNA fingerprinting using the Promega GenePrint® 10 System according to the manufacturer's instructions (Promega #B9510).

2.2 | Antibodies

The following primary antibodies were used for immunoblots and immunofluorescence (IF): anti-SMC2 (A300-056A; Bethyl), anti-SMC4 (ab17958; Abcam), anti-CAPD3 (A300-604A; Bethyl), anti-CAPG2 (A300-605A; Bethyl), anti-CAPH2 (A302-275A; Bethyl), anti-53BP1 (ab38623; Abcam), anti-γH2AX (05-636; EMD Millipore), anti-tubulin (T9026; Sigma), anti-actin (A5441; Sigma), anti-myc-tag (2272; Cell Signaling), anti-Histone H3 (ab1791; Abcam), and anti-GFP (632381; Takara Bio).

2.3 | Plasmid constructs

Myc-tagged WT CAPH2 protein was expressed from pCS2-myc-CAPH2 (Wallace et al., 2019). QuikChange II XL Site-directed mutagenesis Kit (Agilent Technologies) was used to introduce the R551P (CGT → CCT), R551S (CGT → AGT), and S556F (TCC → TTC) point mutations into pCS2-myc-CAPH2. The T2A-EGFP sequence (Kim et al., 2011; Figure 1) was cloned into the AscI site directly following CAPH2 in pCS2-myc-CAPH2, and the stop codon of CAPH2 was removed by site-directed mutagenesis.

2.4 | Cell cycle analysis

RPE1 cells were transfected with small interfering RNA (siRNA) or expression constructs and fixed with 70% ethanol after 48 h. DNA was stained with the FxCycle PI/RNase Staining Solution (molecular probes by Life Technologies) according to the manufacturer's instructions, and DNA content was quantified with a MACSQuant VYB flow cytometer. Data were analyzed with FlowJo, using the Dean-Jett Fox model to estimate cell cycle proportions.

2.5 | Annexin staining

Cells were plated in six-well plates and harvested by trypsinization without fixing. Annexin staining was performed using the Alexa Fluor 488 Annexin V/Dead Cell Apoptosis Kit from Molecular Probes and quantified with a MACSQuant VYB flow cytometer, with at least 10,000 cells counted per sample.

2.6 | siRNA and overexpression construct transfection

CAPH2 siRNA #1 was NCAPH2 siGENOME SMARTpool (M-016186-01) from Dharmacon, and CAPH2 #2 siRNA was a 1:1 mixture of the following two custom duplexes from Dharmacon (sense): CUGAUGAAAUGGAGAAGAAUU and ACAGUAAGAAG GUGGAAUAUU. Other siRNAs used were as follows: siGENOME SMARTpool siRNA for ataxia telangiectasia and Rad3-related (ATR; M-003202-05), ON-TARGETplus SMARTPOOL siRNA for ataxia-telangiectasia mutated (ATM; L-003201-00), and siGENOME non-targeting siRNA Pool #2 (D-001206-14) for negative control. Cells were nucleofected with 300 pmol of each siRNA or 2 μg of overexpression plasmid using the Nucleofector II device and Amaxa Cell Line Nucleofector Kit V (program #I-013 for RPE1, and D-032 for HCT116).

2.7 | Immunoblot

After harvesting by scraping, cells were frozen at −80°C for at least 10 min, lysed in 3-[(3-cholamidopropyl)dimethylammonio]-1-propanesulfonate (CHAPS) buffer (0.5% weight/volume CHAPS, 10% glycerol, 5 mM $MgCl_2$, and 1 mM EDTA in 50 mM Tris-HCl, pH 7.5) for 15 min on ice, and centrifuged at 20,000*g* for 15 min. The supernatant was isolated as the whole-cell soluble fraction. Two different methods were employed to isolate chromatin-bound

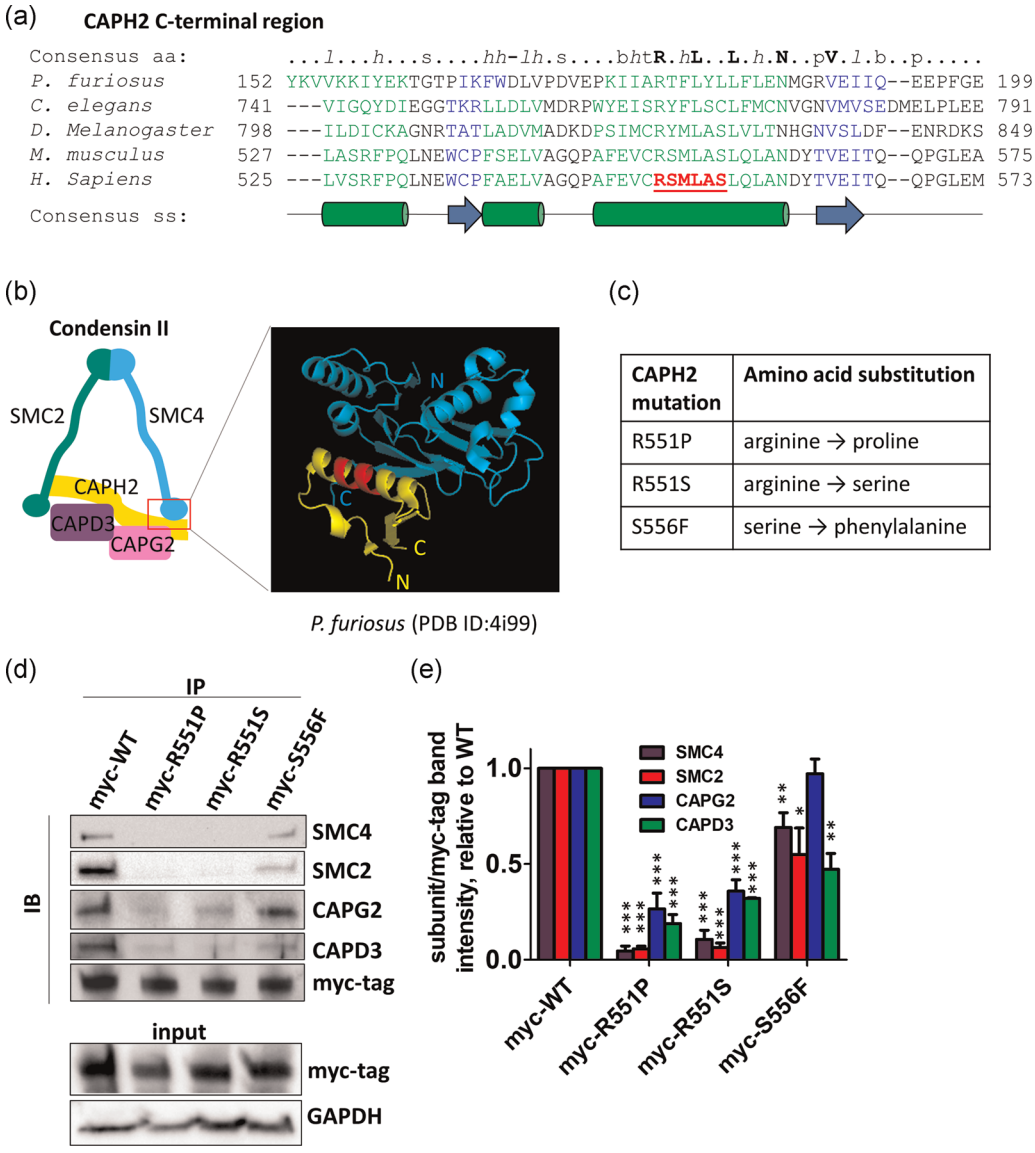

FIGURE 1 R551P, R551S, and S556F mutations in CAPH2 are located in the α-helix that binds SMC4 and cause decreased binding of CAPH2 to other condensin II subunits. (a) Multisequence alignment of a C-terminal region of CAPH2. The region containing a significant cluster of missense mutations is indicated in red. Green cylinders indicate α-helices, blue arrows indicate β-sheets. (b) Crystal structure of the Smc Head (blue) bound to the winged-helix domain of ScpA (yellow) in *Pyrococcus furiosus*. The region containing a significant cluster of missense mutations is indicated in red. (c) R551P, R551S, and S556F amino acid substitutions. (d) RPE1 cells were transfected with myc-tagged mutant or wild-type (WT) CAPH2 constructs. Cells were harvested after 24 h, coimmunoprecipitation (co-IPs) was performed with myc-tag antibody, and the lysates were immunoblotted. (e) Quantification of immunoblots. Two–three co-IPs were performed per construct and averaged. aa, amino acid; ss, secondary structure. $^{*}p < .05$, $^{**}p < .01$, $^{***}p < .001$, two-tailed unpaired *t*-test. Error bars = *SEM*

proteins (Figure 2e), a high-salt buffer method for immunoblotting myc-tagged CAPH2, SMC4, and CAPG2, and a sodium dodecyl sulfate (SDS) buffer method for immunoblotting CAPD3 and SMC2. The high-salt buffer method is a more stringent method for isolating only chromatin-bound proteins, but CAPD3 and SMC2 bands were undetectable by this method, and so the SDS buffer method was followed. For both methods, the cells were lysed as above to remove the whole-cell soluble fraction. The remaining pellet was then incubated with Turbo DNase for 20 min at room temperature (RT), and centrifuged at 20,000*g* for 3 min. For the high-salt method, the remaining pellet was incubated in high-salt lysate buffer (20 mM Tris, pH 7.5, 500 mM KCl, 300 mM sucrose, 5 mM $MgCl_2$, 1 mM EDTA, 0.5% NP40, 2 mM ATP) for 15 min on ice, pelleted at 20,000*g*, and the supernatant was combined with the supernatant from DNase treatment. For the SDS buffer method, the remaining pellet after DNase treatment was dissolved with SDS buffer (120 mM Tris, pH 6.8, 4% SDS, 20% glycerol), pelleted at 20,000*g*, and the supernatant was combined with the supernatant from DNase treatment. All protein samples were boiled for 10 min in Laemmli buffer, resolved by SDS–polyacrylamide gel electrophoresis on a 4%–15% gel,

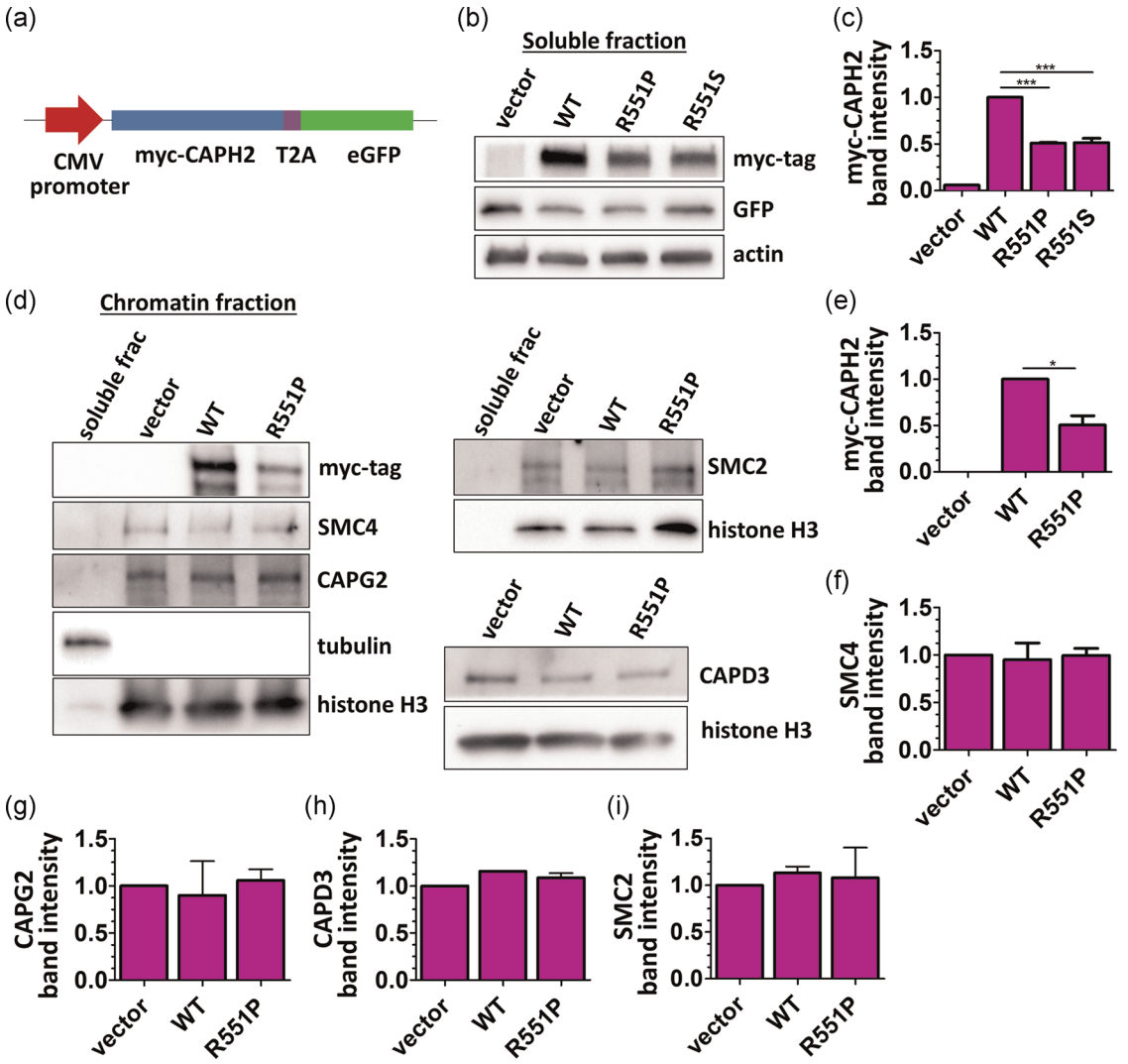

FIGURE 2 R551P mutant CAPH2 protein exhibits decreased protein stability and decreased binding to chromatin. (a) Expression construct used to express CAPH2 and EGFP. Both CAPH2 and EGFP are expressed separately from the same messenger RNA transcript, allowing the use of EGFP as a normalization factor for CAPH2 transcription. (b) RPE1 cells were harvested 24 h after plasmid transfection of expression constructs, and soluble fraction lysates were immunoblotted. (c) Quantification of soluble fraction myc-tag band intensity normalized to EGFP band intensity, relative to wild-type (WT). (d) Immunoblots of the chromatin-bound fraction. (e–i) Quantification of chromatin fraction band intensities normalized to histone H3 band intensity, relative to WT. Two or three westerns were averaged in each quantification. $^{*}p < .05$, $^{**}p < .01$, $^{***}p < .001$, two-tailed unpaired *t*-test. Error bars = *SEM*

transferred to a nitrocellulose membrane, and blocked in PBS-T (PBS with 0.05% Tween20) with 5% milk. Primary antibodies listed in Section 2.2 were incubated with the membrane overnight at 4°C. Horseradish peroxidase-conjugated secondary antibodies were used for chemiluminescent imaging. Blots were imaged on a ChemiDoc (BioRad).

2.8 | Coimmunoprecipitation

Myc-tagged proteins were coimmunoprecipitated with the Pierce Magnetic c-Myc-Tag IP/co-IP Kit (88844; Thermo Fisher Scientific) according to the manufacturer's instructions. Beads were incubated with lysates overnight at 4°C.

2.9 | Immunofluorescence

Cells on coverslips in 12-well plates were washed once with phosphate-buffered saline (PBS) and fixed with 4% paraformaldehyde (PFA) in PBS for 10 min. Cells were permeabilized with PBS + 0.5% Triton X-100, washed in PBS + 0.1% Triton X-100, and blocked in 5% bovine serum albumin (BSA) in PBS + 0.1% Triton X-100. Coverslips were incubated with primary antibodies (see Section 2.2) at 1:500 overnight at 4°C in blocking solution. After washing, the coverslips were incubated with secondary antibody (Alexa488 conjugated anti-rabbit or anti-mouse; Jackson Laboratories) at 1:500 for 1 h at RT. Nuclei were stained with 4′,6-diamidino-2-phenylindole (DAPI) and coverslips were mounted with Vectashield Mounting Medium (Vector Laboratories). DNA damage foci were imaged on a

Nikon Eclipse E800 with an Olympus DP controller with a ×20 lens. At least three fields of view were chosen from which to count foci. Foci were counted using the Find Maxima feature of ImageJ with a noise threshold of 15. Anaphase defects were imaged on a Nikon Eclipse Ti with a ×60 oil immersion lens. Anaphase defects images in Figure 2a are Max Intensity Projections of 5-7 z-stack slices, 0.25 µm step size.

2.10 | 5-Ethynyl-2′-deoxyuridine staining with γH2AX IF

Cells were transfected and plated on coverslips in 12-well plates. At 48 h posttransfection cells were pulsed for 30 min with 10 uM 5-ethynyl-2′-deoxyuridine (EdU) using the Click-iT™ EdU Cell Proliferation Kit for Imaging with Alexa Fluor™ 555 dye from Thermo Fisher Scientific (C10338). Coverslips were then fixed with 4% PFA in PBS for 10 min and processed according to kit instructions. After processing coverslips were washed twice with 1% BSA in PBS and IF was performed as detailed above in Section 2.9, beginning with the permeabilization step and using anti-γH2AX antibody (05-636; EMD Millipore).

2.11 | DNA fluorescence in situ hybridization for CIN assay

DNA fluorescence in situ hybridization (FISH) probes for the centromeric α-satellite regions of chromosome 8 and chromosome 12 were purchased from Cytocell (LPE008G and LPE012R). DNA FISH was performed according to the manufacturer's instructions. Briefly, cells were incubated in 75 mM KCl for 15 min at 37°C, fixed in 3:1 methanol:acetic acid, and dropped onto a slide. Slides were immersed in 2X saline-sodium citrate (SSC) buffer and dehydrated in an ethanol series (70%, 85%, 100%). Slide samples and probes were denatured at 75°C for 2 min, and hybridization took place overnight at 37°C. After hybridization slides were washed in 0.25X SSC at 72°, then in 2X SSC with 0.05% Tween-20 and DAPI at RT. Coverslips were mounted with Vectashield. Interphase cells were imaged on a Nikon Eclipse E800 with an Olympus DP controller with a ×20 lens.

2.12 | DNA FISH for telomere- and centromere-containing anaphase bridges

FISH probes were obtained from PNA Bio (TelC-Cy3 probe: F1002; CENPB-FAM probe: F3001). DNA FISH was performed according to the manufacturer's instructions. Briefly, coverslips were dehydrated in an ethanol series (70%, 85%, 100%). Coverslips and 500 nM probe in hybridization buffer were preheated at 85°C for 5 min, probe solutions were added to the coverslips and heated at 85°C for 10 min, and hybridization took place at RT for 4 h. After hybridization slides were washed in 2X SSC with 0.1% Tween-20 at 60°C, then in 2X SSC with DAPI. Coverslips were mounted with Vectashield. Anaphase bridges were imaged with a ×60 oil immersion lens on a Nikon Eclipse Ti, with z-stack slices of 0.25 µm. Slices were observed manually from the top of the bridge to the bottom for centromere or telomere foci. Anaphase bridge images in Figure 3d are maximum intensity projections of 5–7 z-stack slices, 0.25 µm step size.

2.12.1 | IF-FISH and telomere dysfunction-induced foci assay

Cells on coverslips in 12-well plates were washed once with PBS and fixed with 4% PFA in PBS for 10 min. Cells were permeabilized with PBS + 0.5% Triton X-100, washed in PBS + 0.1% Triton X-100, and blocked in 5% BSA in PBS + 0.1% Triton X-100. Coverslips were incubated with γH2AX primary antibody (see Section 2.2) at 1:500 overnight at 4°C in blocking solution. After washing, the coverslips were incubated with secondary antibody (Alexa488 conjugated anti-mouse; Jackson Laboratories) at 1:500 for 1 h at RT. Coverslips were washed with PBS + 0.1% Triton X-100, and postfixed with 4% formaldehyde in 1X PBS for 10 min. The TelC-Cy3 FISH probe (F1002) was obtained from PNA Bio. FISH was performed according to the manufacturer's instructions. Briefly, coverslips were dehydrated in an ethanol series (70%, 85%, 100%). Coverslips and 500 nM probe solutions were preheated at 85°C for 5 min, probe solutions were added to the coverslips and heated at 85°C for 10 min, and hybridization took place at RT for 4 h. After hybridization slides were washed in 2X SSC with 0.1% Tween-20 at 60°C, then in 2X SSC with DAPI. Coverslips were mounted with Vectashield. Nuclei were imaged with a ×60 oil immersion lens on a Nikon Eclipse Ti, with z-stack slices of 0.25 µm. Slices were observed manually from the top of the nucleus to the bottom for foci with red and green colocalization. telomere dysfunction-induced foci (TIF) images in Figure 3a are Max Intensity Projections of 5–7 z-stack slices, 0.25 µm step size.

2.13 | Statistics

Unpaired Student's *t*-test was used for statistical analysis with a *p*-value of less than .05 as the criteria for a significant difference. Statistical data were calculated with GraphPad Prism.

3 | RESULTS

3.1 | Cancer-associated mutations in CAPH2 are located in the SMC4 binding region and cause decreased binding to other condensin II subunits

Computational network analysis identified condensin I & condensin II complex subunits as being significantly mutated in multiple cancer types, with 4.2% of the samples analyzed having condensin

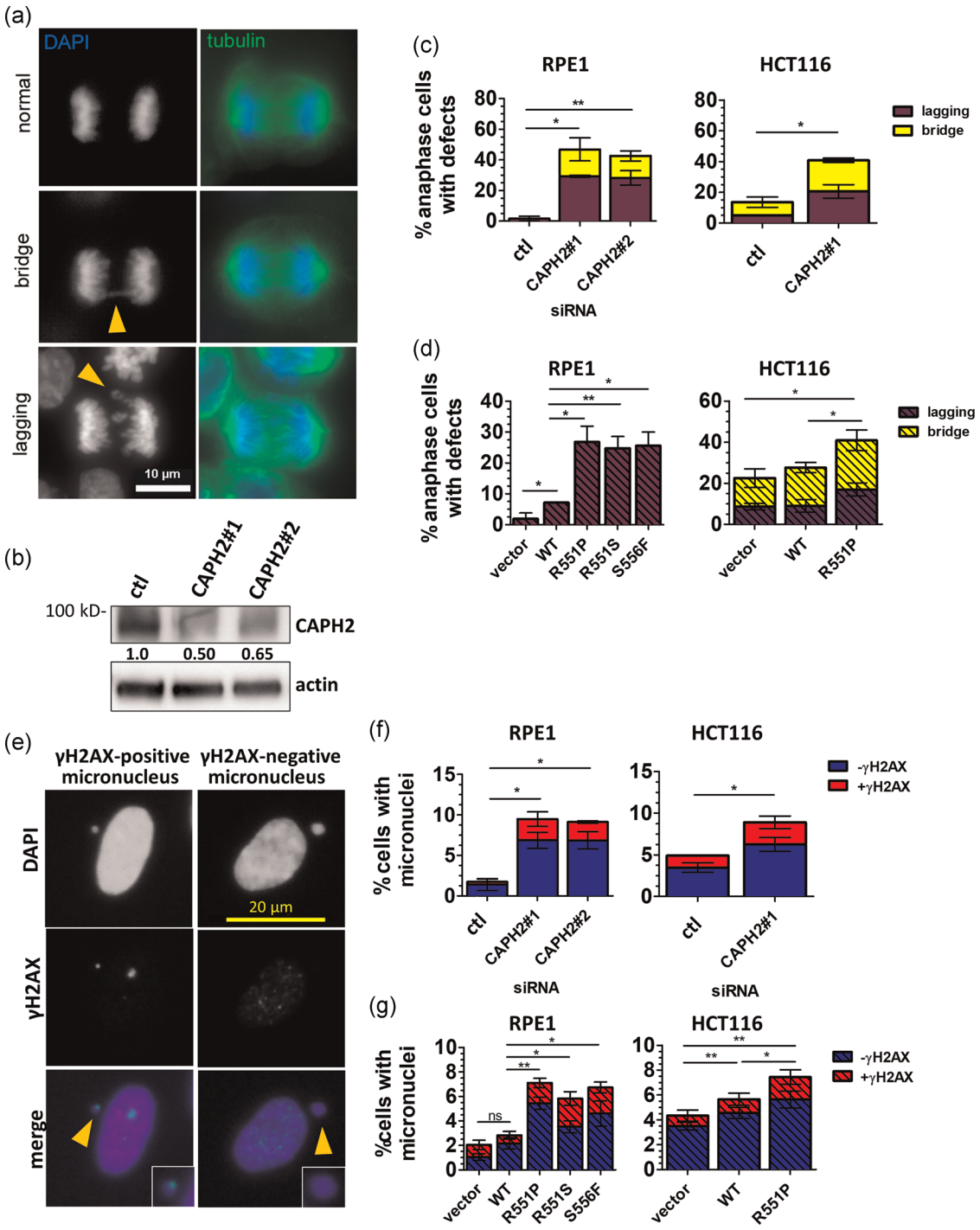

FIGURE 3 Expression of R551P, R551S, and S556F CAPH2 proteins causes anaphase defects and micronuclei. (a) Representative immunofluorescence microscopy images of anaphase defects in HCT116 cells. Yellow arrowheads mark defects. (b) HCT116 cells were transfected with small interfering RNA (siRNA), harvested after 48, and immunoblotted. (c, d) Quantification of anaphase defects in either RPE1 or HCT116 cells transfected with siRNA (c) or expression constructs (d) and fixed at 48 h. (e) Representative immunofluorescence microscopy images of micronuclei. Yellow arrowheads mark micronuclei. (f, g) Quantification of micronuclei in RPE1 or HCT116 cells transfected with siRNA (f) or expression constructs (g) and fixed at 48 h. To aid visualization, graphs with siRNA knockdown are depicted with open bars and graphs with CAPH2 overexpression are depicted with diagonal crosshatches. Statistics were performed for the overall number of anaphase defects or micronuclei, disregarding the type of defect or γH2AX positivity. See Figure S4 for additional significance tests not displayed on graphs. DAPI, 4′,6-diamidino-2-phenylindole; WT, wild-type. $^{*}p < .05$, $^{**}p < .01$, $^{***}p < .001$, two-tailed unpaired *t*-test. Error bars = *SEM*

mutations (Leiserson et al., 2015). A significant cluster of missense mutations was discovered in a C-terminal region of the condensin II subunit CAPH2 (Leiserson et al., 2015). To understand how these condensin II mutations may contribute to cancer, we set out to characterize the three mutations found in this cluster: R551P, R551S, and S556F. CAPH2 is a member of the kleisin family of proteins, which are conserved from bacteria to humans. The C-terminus of CAPH2 contains a winged-helix domain (WHD) that binds to the head of SMC4 (Burmann et al., 2013). Alignment of CAPH2 with kleisin subunits from other species revealed that R551P, R551S, and S556F are located in the middle of a WHD helix (Figure 1a). The crystal structure of the analogous helix in the bacteria *Pyrococcus furiosus* (PDB ID: 4i99) demonstrates that this helix makes direct contact with the SMC head (Figure 1b). Therefore, it is highly likely that R551P, R551S, and S556F are located in a region of CAPH2 that binds directly to SMC4. Of the three CAPH2 missense mutations, R551P is predicted to have the largest effect on helix structure (Figure 1c), as proline's R-group cannot participate in hydrogen bonding and could introduce a kink into the WHD helix.

The predicted location of the R551P, R551S, and S556F CAPH2 mutations in the binding region for SMC4 raise the possibility that these mutations disrupt CAPH2-SMC4 binding. To determine the effect of the R551P, R551S, and S556F CAPH2 mutations on binding to SMC4 and other condensin II subunits, myc-tagged WT and mutant CAPH2 proteins were expressed in non-transformed human telomerase-immortalized RPE1 cells (Bodnar et al., 1998). IF demonstrated that WT and mutant CAPH2 proteins were expressed and localized to the nucleus (Figure S1a). Expression of WT and mutant CAPH2 proteins, or knockdown of CAPH2 with siRNA, did not alter the cell cycle after 48 h (Figure S1b,c). Annexin staining indicated that expression of R551P CAPH2 did lead to a small but significant increase in apoptotic cells (Figure S1d).

Coimmunoprecipitations (co-IPs) were performed to determine the extent to which each of the expressed myc-tagged proteins physically interacted with other condensin II complex subunits (Figure 1d,e). In comparison to WT CAPH2, each of the three mutated proteins exhibited decreased levels of other condensin II subunits in the co-IPs. The R551P and R551S mutations abolished CAPH2 binding to SMC2 and SMC4 (Figure 1d,e). Additionally, CAPH2 binding to both CAPG2 and CAPD3 was decreased by ~80% ($p < .001$) for R551P and ~75% ($p < .001$) for R551S mutants. The S556F mutation had a less severe impact on condensin II subunit interactions, but it still decreased CAPH2 binding to SMC2, SMC4, and CAPD3 by ~50% ($p < .05$). These data indicate that R551P, R551S, and S556F CAPH2 mutations not only disrupt the binding of CAPH2 to SMC4, as was predicted but in fact decrease CAPH2 binding to all the members of the condensin II complex and presumably impede assembly into a complex. To our knowledge, this is the first report of condensin mutations from human clinical samples that have a functional consequence on condensin complex formation.

3.2 | R551P mutant CAPH2 protein exhibits decreased protein stability and decreased binding to chromatin

After determining that the R551P, R551S, and S556F CAPH2 mutants are less efficient at binding other condensin complex subunits, we wondered if these mutations caused decreased CAPH2 mutant protein stability. The mutations could cause increased protein turnover. Additionally, previous reports have observed that depletion of one condensin subunit leads to a decrease in protein levels of other subunits, and it has been suggested that stoichiometric changes that lead to condensin subunits not being incorporated into complexes cause degradation of the unincorporated subunits (George et al., 2014; Hirota et al., 2004). To determine if the mutations affected CAPH2 protein stability, myc-tagged CAPH2 proteins were overexpressed from a plasmid containing a T2A EGFP sequence (Figure 2a). This bicistronic vector creates one messenger RNA (mRNA) from which both CAPH2 and EGFP are separately translated, allowing the use of EGFP as a normalization factor for CAPH2 transcription. We transfected the WT and mutant myc-CAPH2-T2A-EGFP constructs into the nontransformed immortalized RPE1 cell line and the colon cancer cell line HCT116, which stably segregates chromosomes and is near-diploid (Thompson & Compton, 2008). Cells were harvested 24 h after transfection. Immunoblotting of cell lysates demonstrated that EGFP was expressed equally for each WT or mutant transfection, indicating that the efficiency of CAPH2 transcription and mRNA translation was equivalent in each condition. In comparison to WT CAPH2, mutant CAPH2 proteins were decreased in the soluble cell fraction, which includes both cytoplasmic and nuclear proteins, by about ~50% ($p < .01$; Figure 2b). R551P and R551S CAPH2 were also decreased in the soluble fraction in HCT116 cells in comparison to WT CAPH2 (Figure S2a,b). Similar to the soluble fraction, in the chromatin fraction of RPE1 cells R551P mutant CAPH2 was decreased by ~50% ($p < .05$; Figure 2d,e). However, the other four subunits of the condensin II complex, SMC4, SMC2, CAPG2, and CAPD3, did not show a detectable difference in protein level when WT or mutant CAPH2 proteins were overexpressed (Figures 2d and 2f–i). We were unable to calculate the effects of CAPH2 overexpression on endogenous CAPH2 levels, as overexpression of CAPH2 resulted in the appearance of a secondary band, likely due to the expression of a CAPH2 isoform or cleavage product, that was at the same molecular weight as endogenous CAPH2 (Figure S2c). Collectively these data demonstrate that R551P CAPH2 is less stable than WT CAPH2 at the protein level and has decreased binding to chromatin.

3.3 | R551P, R551S, and S556F CAPH2 mutations cause anaphase defects and micronuclei

The most well-documented function of condensin II is to condense chromatin during mitosis (George et al., 2014; Green et al., 2012;

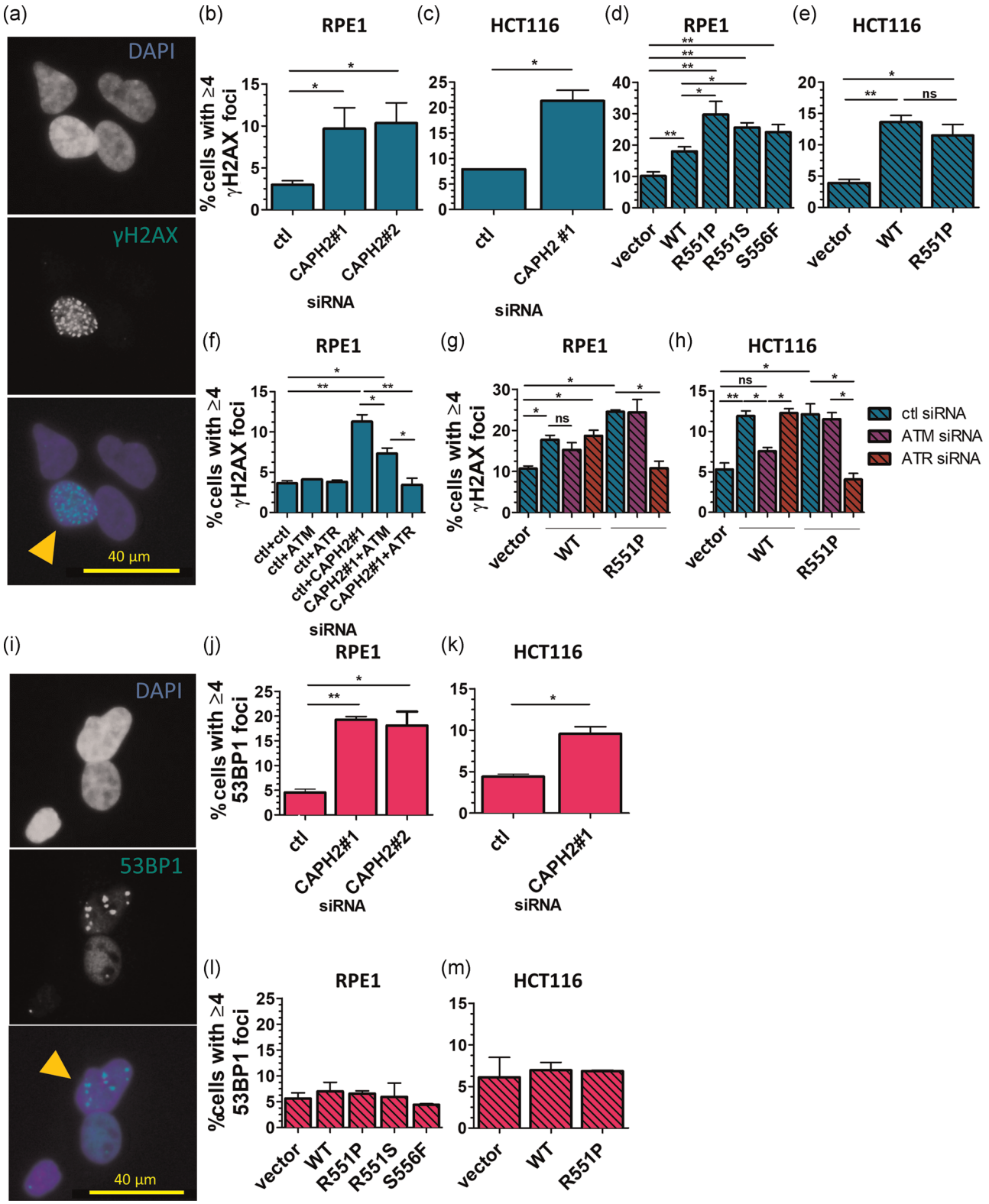

FIGURE 4 (See caption on next page)

Hirota et al., 2004; Martin et al., 2016; Woodward et al., 2016). Cells with decreased condensin II subunit expression or defective condensin II activity exhibit mitotic anomalies such as anaphase defects (Green et al., 2012; Martin et al., 2016; Woodward et al., 2016). CAPH2 mutations lead to decreased mutant CAPH2 protein levels and compromised ability to interact with other condensin II subunits (Figure 2), suggesting that mutant proteins may behave as recessive loss-of-function mutations with no phenotypic consequence.

Alternatively, assembly of mutant CAPH2 into condensin II complexes or the presence of mutant CAPH2 on chromatin could affect the activity and/or localization of condensin II complexes. In this latter scenario, we considered the possibility that expression of the R551P, R551S, and S556F mutant CAPH2 would behave as dominant mutations and compromise the activity of condensin II and cause an increase in anaphase defects. To test these two possibilities RPE1 and HCT116 cells were transfected with CAPH2 siRNA, or WT and mutant CAPH2 expression constructs, and fixed after 48 h. Immunofluorescent staining with a tubulin antibody was used to visualize the mitotic spindle, and DNA was stained with DAPI. The presence of chromatin bridges and lagging chromosomes were scored in anaphase cells (Figure 3a). CAPH2 siRNA knockdown caused an increase in cells with anaphase defects in both RPE1 and HCT116 cells (Figure 3b,c). Expression of WT CAPH2 in RPE1 cells caused an increase in cells with anaphase defects, but not in HCT116 cells (Figure 3d). In RPE1 cells, expression of R551P, R551S, or S556F CAPH2 protein caused a significant increase in cells with anaphase defects relative to cells transfected with vector alone or vector expressing WT CAPH2 (Figure 3d). In HCT116 cells expression of R551P CAPH2 protein also caused a significant increase in cells with anaphase defects relative to cells transfected with vector alone or vector expressing WT CAPH2. Interestingly, mutant CAPH2 expression in RPE1 caused cells to exhibit only lagging chromosomes, whereas siRNA depletion produced both lagging chromosomes and chromosome bridges (Figure 3c,d).

Anaphase defects, including lagging chromosomes, can lead to micronuclei. Because micronuclei can be generated from chromosome missegregation in anaphase (Crasta et al., 2012), and CAPH2 mutant expression causes elevated levels of anaphase defects (Figure 3a–d), we wondered if mutant CAPH2 expression could lead to the formation of micronuclei. Micronuclei are double-membraned structures outside of the main nucleus that contains whole chromosomes or chromosome fragments. Micronuclei form from genomic material that fails to segregate with one of the two masses of chromosomes during mitosis and persists into G1-phase physically separated and visibly distinct from a cell's main nucleus (Fenech et al., 2011). In subsequent cell cycles, DNA within micronuclei can undergo DNA damage and/or additional fragmentation and then reintegrate into the main nucleus, potentially incorporating mutations and chromosomal rearrangements into the genome (Crasta et al., 2012; Hatch et al., 2013). Damaged or fragmented DNA inside micronuclei may cause chromothripsis observed in cancer cells, in which hundreds to thousands of genomic rearrangements are linked back to a single catastrophic event (Umbreit et al., 2020; Zhang et al., 2013, 2015). We used immunofluorescent staining to look for the presence of micronuclei in RPE1 and HCT116 cells. Cells were transfected with CAPH2 siRNA, or WT and mutant CAPH2 overexpression constructs, and fixed after 48 h. Immunofluorescent staining with a γH2AX antibody was used as a marker for DNA damage, and DNA was stained with DAPI (Figure 3e). CAPH2 knockdown caused an increase in cells with micronuclei in both RPE1 and HCT116 cells (Figure 3f). Overexpression of WT CAPH2 caused an increase in micronuclei in HCT116 cells, but not in RPE1 cells (Figure 3g). In RPE1 cells, overexpression of R551P, R551S, or S556F CAPH2 protein caused a significant increase in micronuclei over cells transfected with vector alone or vector expressing WT CAPH2. Overexpression of R551P CAPH2 in HCT116 cells also caused an increase in cells with micronuclei over cells transfected with vector alone or vector overexpressing WT CAPH2. Taken together with the anaphase defects, these data suggest that one consequence of the increase in anaphase defects in cells expressing R551P, R551S, or S556F CAPH2 is an increase in micronuclei, a proportion of which contain DNA damage, which may in subsequent mitoses be reincorporated into the main nucleus.

3.4 | R551P, R551S, and S556F CAPH2 mutations cause DNA damage

As the expression of R551P, R551S, and S556F proteins causes mitotic defects, we next tested whether expression of these mutant proteins has an impact on cells in interphase by probing for γH2AX foci, a marker of DNA damage. γH2AX, or phosphorylated histone H2AX, is phosphorylated by the kinases ATM and ATR in response to DNA damage (Marechal & Zou, 2013). Thus, the number of γH2AX foci in the cell is representative of the amount of DNA damage, while the activity of ATR or ATM required to produce γH2AX foci is reflective of the type of DNA damage. RPE1 and HCT116 cells were transfected with CAPH2 siRNA, or WT and mutant CAPH2

FIGURE 4 Expression of R551P, R551S, and S556F CAPH2 proteins causes DNA damage. (a) Representative immunofluorescence microscopy images of γH2AX foci. Yellow arrowheads mark cells with ≥4 foci. (b, c) Quantification of γH2AX foci in RPE1 (b) or HCT116 (c) cells transfected with small interfering RNA (siRNA) and fixed at 48 h. (d, e) Quantification of γH2AX foci in RPE1 (d) or HCT116 (e) cells transfected with expression constructs and fixed at 48 h. (f) Quantification of γH2AX foci in RPE1 cells transfected with two siRNAs. Cells were fixed 48 h posttransfection. (g, h) Quantification of γH2AX foci in RPE1 (g) or HCT116 (h) cells transfected with one siRNA (indicated by bar color) and one expression construct. Cells were fixed 48 h posttransfection. (i) Example immunofluorescence microscopy images of 53BP1 foci. Yellow arrowheads mark cells with ≥4 foci. (j, k) Quantification of 53BP1 foci in RPE1 (j) or HCT116 (k) cells transfected with siRNA and fixed at 48 h. (l, m) Quantification of 53BP1 foci in RPE1 (l) or HCT116 (m) cells transfected with expression constructs and fixed at 48 h. To aid visualization, graphs with siRNA knockdown are depicted with open bars and graphs with CAPH2 overexpression are depicted with diagonal crosshatches. See Figure S5 for additional significance tests not displayed on graphs. DAPI, 4′,6-diamidino-2-phenylindole; WT, wild-type. $^{*}p < .05$, $^{**}p < .01$, $^{***}p < .001$, two-tailed unpaired *t*-test. Error bars = *SEM*

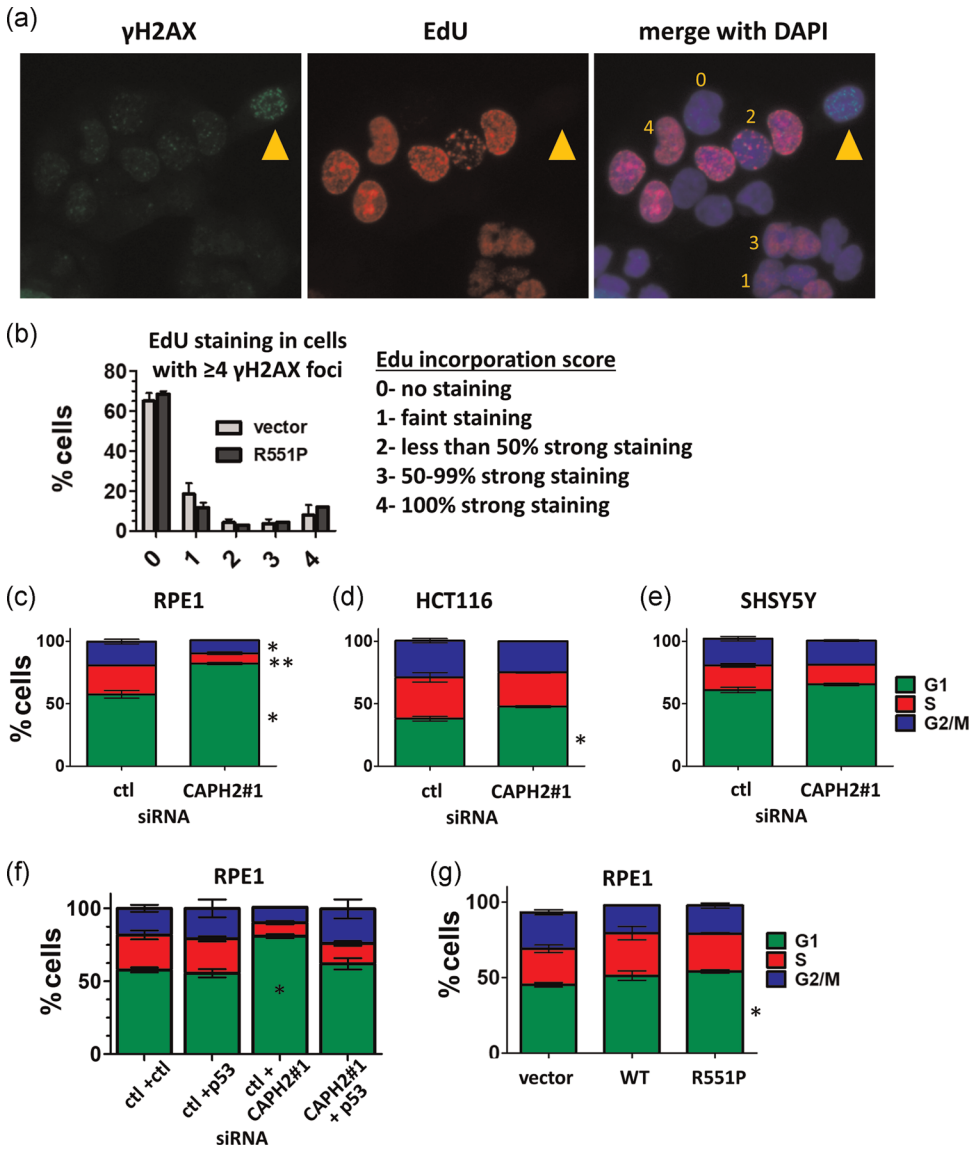

FIGURE 5 R551P CAPH2 causes DNA damage outside of S-phase. (a) Representative immunofluorescence microscopy images of 5-ethynyl-2′-deoxyuridine (EdU) staining and γH2AX foci in RPE1 cells. Yellow arrowhead marks a cell with ≥4 γH2AX foci. Yellow numbers are example scores for the quantitation system described in (b). b) Quantification of EdU staining in RPE1 cells with ≥4γH2AX foci. Cells were transfected with expression constructs, and pulsed with EdU for 30 min immediately before fixation at 48 h after transfection. EdU staining was scored from 0 to 4 using the indicated system, where 0 = no detectable EdU incorporation (arrowhead) and 4 = 100% of the nucleus exhibits EdU labeling. (c–e) Cell cycle analysis. Cells were transfected with small interfering RNA (siRNA) and fixed after 4d, DNA was stained with propidium iodide and DNA content was determined with flow cytometry. (f) Cell cycle analysis was performed as above in (c–e) in RPE1 cells transfected with two siRNAs. (g) Cell cycle analysis was performed as above in (c–e) in RPE1 cells transfected with expression constructs. $^{*}p < .05$, $^{**}p < .01$, $^{***}p < .001$, two-tailed unpaired *t*-test. Error bars = *SEM*

overexpression constructs, and cells were fixed after 48 h. Immunofluorescent staining with γH2AX antibody was performed, and DNA was stained with DAPI (Figure 4a). CAPH2 knockdown caused an increase in γH2AX foci in both RPE1 and HCT116 cells (Figure 4b,c). This observation is consistent with previous reports that depletion of condensin levels leads to DNA damage (Wallace et al., 2019). In RPE1 cells, overexpression of WT CAPH2 increased γH2AX foci compared to vector only, and overexpression of mutant CAPH2 proteins caused an even greater increase in DNA damage foci (Figure 4d). In HCT116 cells, overexpression of WT and R551P CAPH2 both increased γH2AX foci to the same amount relative to vector alone (Figure 4e).

To further elucidate the pathway through which DNA damage is occurring, we tested potential kinases involved in H2AX phosphorylation. H2AX is phosphorylated by ATM or ATR depending on the type of DNA damage (Marechal & Zou, 2013). ATM is recruited to DNA damage by the MRN complex and is primarily associated with double-strand breaks (Uziel et al., 2003). ATR is activated by

double-strand breaks and by damage that involves single-stranded DNA (ssDNA) or resected DNA such as stalled replication forks or other replication-associated lesions generating ssDNA. We knocked down ATM and ATR with siRNA to determine which kinase is involved in creating γH2AX foci from CAPH2 knockdown or overexpression of WT or mutant CAPH2. As shown previously (Wallace et al., 2019), the majority of γH2AX foci caused by CAPH2 knockdown in RPE1 cells is dependent on ATR. Here, we observed that γH2AX foci in RPE1 cells with CAPH2 knockdown were also moderately dependent on ATM, but to a lesser extent than ATR (Figure 4f). γH2AX foci in RPE1 cells overexpressing WT CAPH2 were dependent on neither ATM or ATR alone (Figure 4g), suggesting that compensation from the other kinase may occur (Bakr et al., 2015; Cliby et al., 1998; Weber & Ryan, 2015), or that a different kinase such as DNA-PK is involved (Stiff et al., 2004). In contrast, γH2AX foci in HCT116 cells overexpressing WT CAPH2 were dependent on ATM but not ATR (Figure 4h). More importantly, γH2AX foci in both RPE1 and HCT116 cells overexpressing R551P CAPH2 were solely dependent on ATR and not ATM (Figure 4g,h), indicating that the DNA damage caused by overexpression of mutant CAPH2 proteins is likely to be qualitatively different than the DNA damage caused by overexpression of WT CAPH2 protein. These data demonstrate that the γH2AX foci caused by CAPH2 siRNA depletion or mutant CAPH2 overexpression are ATR dependent suggests that the damage may be replication and/or ssDNA related.

To further explore the presence of DNA damage we looked for a second DNA damage marker: 53BP1 foci. 53BP1 is a DNA damage response protein that is phosphorylated and forms foci at double-strand breaks (Zimmermann & de Lange, 2014). Cells were transfected with CAPH2 siRNA, or WT and mutant CAPH2 overexpression constructs, and after 48 h immunofluorescent staining with 53BP1 antibody was performed (Figure 4i). CAPH2 knockdown caused an increase in 53BP1 foci in both RPE1 and HCT116 cells (Figure 4j,k). However, overexpression of WT or mutant CAPH2 in either RPE1 or HCT116 did not cause an increase in 53BP1 foci (Figure 4l,m). Costaining of cells overexpressing R551P CAPH2 with antibodies for 53BP1 and γH2AX confirmed that the majority (95%) of cells that scored positive for γH2AX foci did not score positive for 53BP1 foci (Figure S3). These data indicate that the DNA damage caused by overexpression of WT or mutant CAPH2 is likely to be 53BP1 independent and is distinct from the damage caused by knockdown of CAPH2. As 53BP1 is primarily phosphorylated by ATM in G1 to facilitate nonhomologous end joining (NHEJ; Feng et al., 2015; Isono et al., 2017), the lack of 53BP1 foci upon overexpression of R551P, R551S, or S556F CAPH2 could indicate that the DNA damage caused by overexpression of mutant CAPH2 occurs during replication and signals primarily through ATR.

3.5 | R551P CAPH2 causes DNA damage outside s-phase

The observation that DNA damage caused by siRNA depletion of CAPH2 or by overexpression of R551P CAPH2 mutant is almost entirely ATR dependent (Figure 4g,h) suggests that this DNA damage is a consequence of replication defects in S-phase. However, it is possible that G1 cells inheriting DNA damage from its previous cell cycle can also signal ATR-dependent DNA damage if ssDNA is present. Given the levels of lagging chromosome and anaphase bridges (Figure 3), we speculated that these mitotic defects may cause damage that then persists into the next G1 phase. In this scenario, DNA damage would be expected to trigger a cell cycle delay in G1. To first test the possibility that the DNA damage was occurring during the S phase, we pulse-labeled cells with EdU for 30 min, fixed cells and stained for γH2AX foci and EdU incorporation. EdU is a nucleoside analog, labeling only cells that are actively replicating DNA. Strikingly, of the HCT116 cells with ≥4 γH2AX damage foci following expression of R551P CAPH2, ~65% of them were EdU-negative (Figure 5a,b). Although the distribution of EdU-negative cells with or without γH2AX foci was not significantly different between R551P CAPH2 and control vector-transfected cells, we note that R551P CAPH2 expressing cells suffer two- to three-fold greater DNA damage than control vector-only cells (Figure 4e). This suggested R551P CAPH2 expression was inducing much greater DNA damage, and the majority of the damage was occurring outside of S-phase. We reasoned that if the DNA damage caused arrest or a lag in a certain phase of the cell cycle, then a cell cycle profile might reveal the phase in which such damage was occurring. No changes in cell cycle distribution were detected in RPE1 cells 2d posttransfection of CAPH2 siRNA or WT or mutant CAPH2 expression constructs (Figure S1b,c). However, CAPH2 depletion with RNA interference (RNAi) for 4 days in RPE1 cells led to a dramatic G1 cell cycle delay, in HCT116 cells only a moderate G1 delay was observed, and there was no delay in SHSY5Y neuroblastoma cells (Figure 5c–e). Cells entering G1 with DNA damage persisting from mitosis are known to arrest in G1 (Giunta et al., 2010; Lezaja & Altmeyer, 2018). Because RPE1 cells have intact p53 signaling, we tested whether this G1 delay caused by CAPH2 depletion was p53 dependent. Indeed, in RPE1 cells co-depletion of both CAPH2 and p53 rescued the G1 delay to levels observed in control siRNA or p53-siRNA alone (Figure 5f). Although the expression of R551P mutant CAPH2 in RPE1 cells for 2 days did not alter the cell cycle (Figure S1b), the expression for 4 days caused a significant G1 delay compared to vector control (Figure 5g). Taken together, these observations suggest that loss of condensin II function, either by siRNA depletion or by overexpression of the mutant protein, causes DNA damage, a significant fraction of which is likely to be occurring outside of S-phase and causes G1 delay. Moreover, whether cells experience a G1 delay as a consequence of this DNA damage may depend on cell type and/or whether the cell is normal or cancerous.

3.5.1 | Telomere dysfunction links expression of R551P CAPH2 to DNA damage foci and anaphase bridges

A proportion of the DNA damage foci observed upon CAPH2 knockdown in RPE1 cells are TIFs (Wallace et al., 2019).

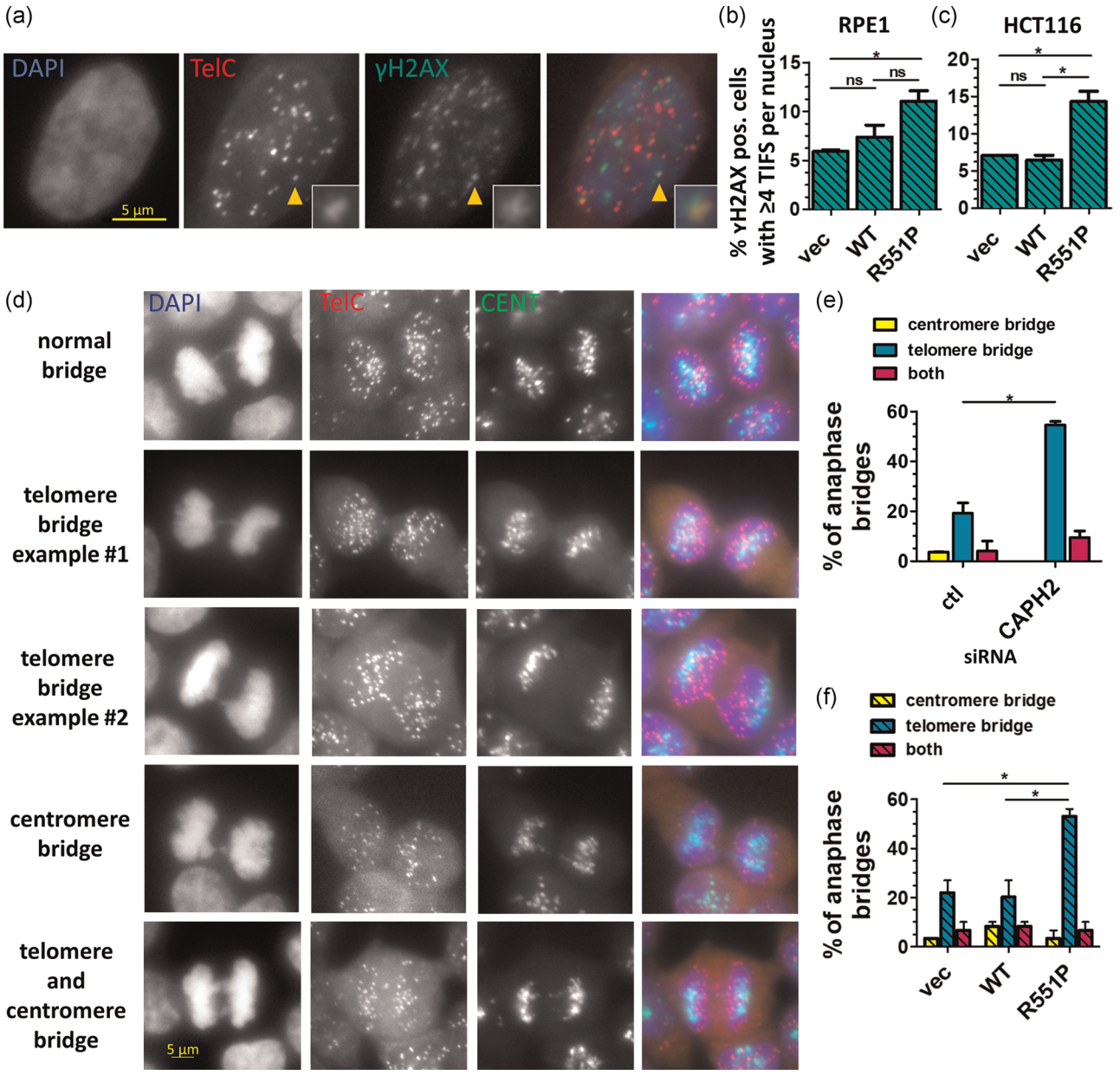

FIGURE 6 Expression of R551P CAPH2 causes an increase in damaged telomeres and an increase in telomere-containing anaphase bridges. (a) Representative immunofluorescence microscopy images of IF-fluorescence in situ hybridization (IF-FISH) in RPE1 cells. (b, c) Quantification of telomere dysfunction-induced foci (TIFs) from IF-FISH. Cells were fixed 48 h after transfection with expression constructs, labeled with a telomere FISH probe (TelC), and probed for γH2AX. Only cells with ≥4γH2AX foci were quantified and represented in the graph. Two biological replicates were performed for each condition, and 70 cells were counted per biological replicate. See Figure S6 for a histogram of the number of TIFs per nucleus. (d) Representative immunofluorescence microscopy images of centromere and telomere FISH in HCT116 cells. Note example number 2 contains multiple telomere signals. (e, f) Quantification of anaphase bridges with centromere or telomere spots from FISH in HCT116 cells. Cells were fixed 48 h after transfection with siRNA (d) or expression constructs (e) and labeled with telomere (TelC) or centromere (CENT) FISH probes. Only cells with anaphase bridges were quantified and represented in the graph. Two biological replicates were performed for each condition, and 30 cells were counted per biological replicate. To aid visualization, graphs with siRNA knockdown are depicted with open bars and graphs with CAPH2 overexpression are depicted with diagonal crosshatches. DAPI, 4′,6-diamidino-2-phenylindole; WT, wild-type. $^{*}p < .05$, $^{**}p < .01$, $^{***}p < .001$, two-tailed unpaired *t*-test. Error bars = *SEM*

TIFs represent activation of the DNA damage response specifically at telomeres and can be caused by short telomeres or loss of shelterin proteins (d'Adda di Fagagna et al., 2003; Cesare et al., 2009; H. Takai et al., 2003). CAPH2 localizes to telomeres and binds to the telomeric shelterin complex subunit TRF1 (Wallace et al., 2019). We used IF-FISH to test if the R551P mutation of CAPH2 would also cause TIF formation. Forty-eight hours after transfection with WT or R551P CAPH2 expression constructs, RPE1 or HCT116 cells were

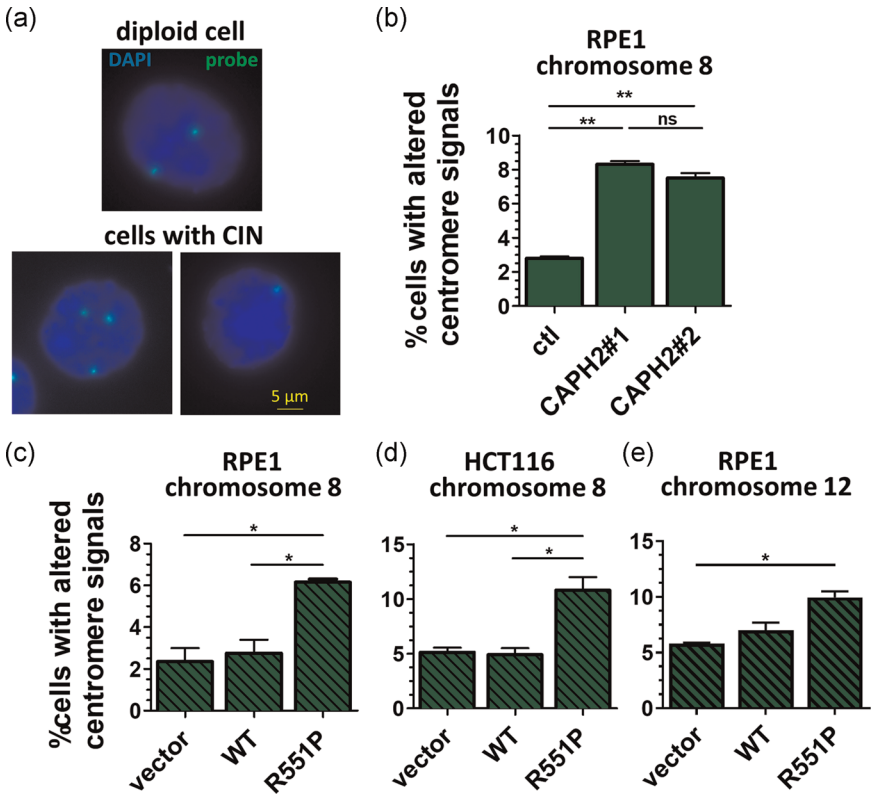

FIGURE 7 Expression of R551P CAPH2 causes an increase in cells exhibiting chromosomal instability (CIN). (a) Representative DNA fluorescence in situ hybridization (FISH) images. DNA FISH was performed with a probe for a centromeric α-satellite region of chromosome 8. Cells with two probe spots were scored as unaltered disomic, and cells with one or three or more probe spots were scored as exhibiting CIN. (b–e) Quantification of cells with altered centromere signals for indicated chromosome in cells with small interfering RNA (siRNA) knockdown of CAPH2 (b) or cells with overexpression of wild-type (WT) and mutant CAPH2 (c–e). To aid visualization, graphs with siRNA knockdown are depicted with open bars and graphs with CAPH2 overexpression are depicted with diagonal crosshatches. Two–three biological replicates were performed for each condition, with at least 100 cells counted per biological replicate. DAPI, 4′,6-diamidino-2-phenylindole. $^{*}p < .05$, $^{**}p < .01$, $^{***}p < .001$, two-tailed unpaired *t*-test. Error bars = *SEM*

fixed, immunostained for γH2AX foci, and probed for telomeres with a FISH probe (Figure 6a). The colocalization of telomeres and γH2AX foci was determined throughout the nucleus. We determined that of cells with ≥4 γH2AX foci, a significantly higher percentage of cells had ≥4 TIFs per nucleus when transfected with R551P CAPH2 versus vector in both cell lines (Figures 6b,c and S6). This is consistent with the results of a similar IF-FISH experiment with CAPH2 knockdown, in which CAPH2 siRNA produced a significantly higher percentage of cells that had greater than 4 TIFs than control siRNA (Wallace et al., 2019).

Telomere dysfunction can also lead to telomere fusions through NHEJ in the case of depletion of shelterin proteins, or Ku-independent microhomology-mediated end-joining in the case of short telomeres (Capper et al., 2007; Smogorzewska et al., 2002). Such fusions are predicted to form dicentric chromosomes that, in anaphase, will form chromosome bridges when the two centromeres are segregating to opposite poles. Moreover, a unique feature of telomere fusions is that some degree of telomeric repeat DNA is expected to be present within the chromosome bridge. To test this possibility, we used DNA FISH to determine if telomere fusions caused the anaphase bridges observed upon expression of R551P mutant CAPH2 in HCT116 cells. Forty-eight hours after transfection with siRNA or WT or R551P CAPH2 expression constructs, HCT116 cells were fixed and probed for centromeres and telomeres with FISH probes (Figure 6d). Centromeres were labeled because condensin knockdown has been shown to cause DNA damage at centromeres in anaphase cells (Samoshkin et al., 2012). We found that the anaphase bridges in HCT116 cells transfected with control siRNA were ~20% telomere-containing bridges, possibly indicating a basal level of telomere dysfunction in this cell line (Figure 6e). However, knockdown of CAPH2 with siRNA more than doubled the percentage of telomere bridges (Figure 6e). Expression of WT CAPH2 did not cause an increase in the percentage of telomere-containing bridges compared to vector, however, expression of R551P mutant CAPH2 led to ~55% of all anaphase bridges to be enriched for telomeric repeat DNA (Figure 6f). There was no change in the percentage of centromere-containing bridges for any of the experimental conditions, arguing that R551P mutant CAPH2 causes anaphase bridges that are likely to arise specifically from telomere dysfunction and DNA damage during interphase.

3.6 | R551P CAPH2 causes increased levels of CIN

CIN is a heightened rate of acquisition of chromosomal abnormalities, causing aberrations such as whole chromosome aneuploidy, translocations, deletions, amplifications, and dicentric chromosomes (Tijhuis et al., 2019). Cells from human microcephaly patients with biallelic NCAPD2 or NCAPD3 mutations (including splice site and frameshift mutations) exhibit increased CIN, as measured by an increase in the percentage of cells with one or three or more DNA FISH spots using a probe for centromeric regions that should only produce two FISH spots for a normal diploid cell (Martin et al., 2016). This observation raises the possibility that in addition to causing DNA damage the cancer-associated CAPH2 mutations could also drive genome instability by causing CIN. Therefore, we tested if CAPH2 knockdown or overexpression of mutant CAPH2 cause CIN by performing DNA FISH with a probe to the centromeric α-satellite region of chromosome 8 or chromosome 12. Forty-eight hours after transfection with CAPH2 siRNA, or WT or R551P CAPH2 expression constructs, cells were fixed and incubated with a FISH probe. Cells were scored as diploid if two spots were visible, and as exhibiting CIN if one, three, or another number of spots were visible (Figure 7a). CAPH2 knockdown in RPE1 caused a significant increase in the percentage of cells exhibiting CIN (Figure 7b). Overexpression of WT CAPH2 did not change the percentage of cells exhibiting CIN in either RPE1 or HCT116 cells. Strikingly, overexpression of R551P CAPH2 protein in both RPE1 and HCT116 caused a significant twofold increase in the percentage of cells exhibiting CIN compared to transfection of vector alone or vector overexpressing WT CAPH2 (Figure 7c–e).

4 | DISCUSSION

It has been suggested through previous work that condensin II functions alone or with other chromatin binding factors to prevent cancer progression. Two factors important for modulating the binding of condensin II to chromatin are the tumor suppressors Rb (Longworth et al., 2008) and MCPH1 (Tervasmaki et al., 2019; Trimborn et al., 2006; Venkatesh et al., 2013; Wang et al., 2014; Yamashita et al., 2011). Rb binds to CAPD3, and Rb is required for proper loading of condensin II onto chromatin (Longworth et al., 2008). Haploinsufficiency of an Rb-E2F1-condensin II complex in Rb mutant tumor cells causes defective chromosome segregation in mitosis and aneuploidy (Coschi et al., 2014). In addition to being associated with primary microcephaly (Martin et al., 2016), MCPH1 is a tumor suppressor that is downregulated in multiple cancer types (Tervasmaki et al., 2019; Venkatesh et al., 2013; Wang et al., 2014). MCPH1 negatively regulates condensin II by competing for binding space on chromatin (Yamashita et al., 2011). Mutations in MCPH1 cause chromosome segregation defects, an increase in micronuclei, and increased CIN (Martin et al., 2016). In addition, the I15N mutation in the murine condensin II subunit CAPH2 leads to the development of T cell lymphoma in a mutant mouse model (Woodward et al., 2016). The I15N mutation causes mitotic defects and DNA damage in T cells (Gosling et al., 2007; Woodward et al., 2016). Finally, the siRNA knockdown of condensin genes is sufficient to alter the number of total chromosomes in a colorectal cancer cell line (Baergen et al., 2019) and trigger BFB cycles capable of generating large-scale genome rearrangements (Umbreit et al., 2020). Here, we characterized the effects of the human cancer-associated mutations R551P, R551S, and S556F (Leiserson et al., 2015), shedding light on why these mutations might give cells a selective advantage during cancer progression. The DNA damage seen in the cells upon overexpression of mutant CAPH2 (Figure 4), together with an increase in anaphase defects (Figure 3d), micronuclei (3 g) and CIN (Figure 7c–e), allow for increased genetic diversity in the tumor cell population. The genomic instability that the R551P, R551S, and S556F CAPH2 mutations create could therefore be a highly favorable facilitator of tumor progression.

Surprisingly, we demonstrate in this study that although the R551P, R551S, and S556F mutations in CAPH2 are located in the binding region for SMC4 (Figure 1a,b), the mutations decrease CAPH2 binding to all of the condensin II subunits (Figure 1d,e). It is possible that the disrupted CAPH2–SMC4 binding causes the entire condensin complex to be released from DNA. This possibility is supported by studies of the *Escherichia coli* condensin complex MukBEF. In this case, impairing the interaction between the CAPH2 kleisin homolog MukF and the SMC homolog MukB, by overexpression of cognate peptides, leads to ATP hydrolysis-dependent release of MukBEF complexes from DNA (Zawadzka et al., 2018). These data suggest that proper CAPH2–SMC4 binding may be necessary to preserve an intact complex and keep condensin II on DNA. However, this possible explanation does not account for the fact that we observe a decrease in chromatin binding only for CAPH2 and not for the other members of the condensin II complex (Figure 2d). Alternative to the release from the chromatin model, it is also possible that the R551P CAPH2 mutation prevents the recruitment of CAPH2 to chromatin. For example, one study reports that Rb binds to CAPD3 and is necessary for the proper loading of CAPD3 onto chromatin (Longworth et al., 2008). Although not explored in that study, Rb may be necessary for the proper loading of the other condensin II complex subunits onto chromatin through binding to CAPD3, in which case lack of binding to CAPD3 by the R551P mutant would prevent CAPH2 from being shuttled to Rb-enriched chromatin. Failure to stably bind chromatin, whether due to release from chromatin or due to insufficient recruitment to chromatin by whatever means, could help explain our finding that the stability of the mutant CAPH2 protein is decreased in both the soluble and chromatin fractions in comparison to WT CAPH2 (Figure 2b). Additionally, CAPH2 protein is stabilized by phosphorylation by the chromatin-associated kinase Plk1 (Kagami et al., 2017). It is possible that mutant CAPH2 with reduced chromatin binding fails to physically interact with Plk1, leading to proteasomal CAPH2 degradation (Kagami et al., 2017).

Although the R551P mutant CAPH2 has limited binding to other condensin II subunits (Figure 1d,e), overexpression of R551P mutant

CAPH2 nevertheless has a similar phenotype to CAPH2 siRNA knockdown in assays for anaphase defects (Figure 3), DNA damage (Figure 4), and CIN (Figure 7). These effects are observed even though endogenous WT CAPH2 is still present in the cells when R551P mutant CAPH2 is overexpressed. To explain our surprising finding that the R551P CAPH2 mutation disrupts the majority of binding to all other condensin II subunits and yet still produces a phenotype, we have three nonmutually exclusive hypotheses. First, it is possible that although R551P CAPH2 does not bind to SMC2 or SMC4, the ~20% binding that it retains to CAPD3 and CAPG2 (Figure 1d,e) sequesters these subunits from endogenous WT complexes. Second, it is possible that CAPH2 binds to chromatin independently of the other condensin II subunits, and that dysfunctional mutant CAPH2 competes for space on chromatin with functional WT CAPH2. Third, it is possible that condensin II forms oligomers and mutant CAPH2 "poisons" these oligomers by binding transiently or weakly to the other subunits of the oligomer. Electron microscopy has indicated that bacterial condensins form high-order oligomers such as extended fibers and rosettes (Fuentes-Perez et al., 2012; Matoba et al., 2005), and other biochemical experiments also suggest the clustering of bacterial condensins (Cui et al., 2008; Woo et al., 2009). Purification of budding yeast condensin also revealed oligomerization, and interestingly only the oligomer fraction demonstrated DNA compaction activity (Keenholtz et al., 2017). Although human condensin oligomerization has not been definitively established, our group previously determined that co-IP of one tagged form of CAPH2 pulled down CAPH2 with a different tag, suggesting the interaction of CAPH2 subunits (fig. S5b of Wallace et al. (2019). If oligomer formation is necessary for proper chromatin compaction and mutant CAPH2 disrupts oligomer formation, then this could explain how the R551P mutant produces a phenotype even in cells with endogenous WT CAPH2.

The mechanism by which DNA damage and TIFs form after loss of condensin II activity remain to be elucidated. Previous studies and this study have demonstrated that CAPH2 localizes to telomeres and binds to the shelterin complex subunits TRF1 and TRF2 (Wallace et al., 2019), that γH2AX foci caused by expression of R551P mutant CAPH2 are dependent on ATR (Figure 4g,h), and that a proportion of these damage foci localize to telomeres (Figure 6f). ATR can be activated at the telomere when the telomere becomes linearized or when shelterin proteins are depleted, deprotecting ssDNA and allowing the ATR-recruiting protein RPA to bind to ssDNA (Denchi & de Lange, 2007; Hockemeyer et al., 2005; de Lange, 2018; Sfeir et al., 2009; K. K. Takai et al., 2011). It is possible that mutant CAPH2 causes TIF formation by decreasing the recruitment of shelterin subunits, such as TRF1 or TPP1-POT1, to telomeres. Because DNA damage induced by condensin depletion or CAPH2 R551P expression is almost entirely ATR dependent (Figure 4g,h), it is reminiscent of defects caused by loss of POT1 (de Lange, 2018). Although we did not directly test whether TPP1-POT1 activity was compromised after condensin loss, the dependency on ATR and recruitment of RPA specifically at telomeres (Wallace et al., 2019) strongly suggests that telomeric ssDNA is the source of damage signaling in condensin deficient cells. However, although it is possible that disruption of TPP1-POT1 ssDNA protection is the cause of telomere damage after condensin loss, we note that POT1 mutations or short hairpin RNA depletion results in telomere fusions only after ~50 cell doublings (Rice et al., 2017), whereas condensin loss produces DNA damage and anaphase bridges after two or three cell doublings (~48 h after transfection). Thus, if TPP1-POT1 function is abrogated as a consequence of condensin loss, then ssDNA and damage foci formation is likely occurring through a molecular mechanism that is different from what has previously been described for TPP1-POT1. Interestingly, siRNA depletion of CAPH2 results in 53BP1 foci whereas in cells expressing the R551P mutant DNA damage foci are free of 53BP1 (Figure 4j–m). This observation was confirmed by additional costaining of cells with 53BP1 and γH2AX (Figure S3). This is in contrast to previous reports of TRF1 and POT1 loss that result in 53BP1 TIFs (Denchi & de Lange, 2007; Sfeir et al., 2009). We suggest that the nature of the DNA damaged sites caused by R551P mutant expression is exclusively ssDNA, and we speculate that 53BP1 is not required at these DNA damage structures and/or 53BP1 is actively inhibited at these sites to promote resectioning. For example, DNA damaged caused by R551P may trigger BRCA1 and PARP2 inhibition of 53BP1 activity that normally blocks resection and generation of ssDNA (Densham et al., 2016; Fouquin et al., 2017; Isono et al., 2017). Whatever the mechanism by which DNA damage and TIFs form after loss of condensin II activity, this study reveals that mutation of CAPH2 is a novel means through which telomeres can become dysfunctional and lead to genome instability in human cancer cells.

Determining the phase of the cell cycle in which γH2AX foci and TIFs are produced after the loss of CAPH2 activity could provide insights into the mechanistic basis of how these foci occur. Our data indicate that cells with ≥4 γH2AX foci are not enriched in S-phase (Figure 5a,b), and that knockdown of CAPH2 or expression of R551P mutant CAPH2 causes G1 arrest/delay (Figure 5c–g). RNAi depletion of CAPH2 causes RPA recruitment to telomeres (Wallace et al., 2019), indicating a role for condensin II in preventing ssDNA formation at telomeres. It is possible that ssDNA present at telomeres leads to sister chromatid telomere fusions observed after depletion of CAPH2 (Wallace et al., 2019), and that these fusions cause chromosome breakages during mitosis that are inherited as damaged DNA in G1 of the next cell cycle (Giunta et al., 2010; Lezaja & Altmeyer, 2018). DNA damage upon depletion of CAPH2 or expression of R551P CAPH2 could also occur in both S-phase and during mitosis, as multiple different processes could be affected at different points in the cell cycle.

Overexpression of WT CAPH2 is interesting clinically because the overexpression of condensin II subunits has been observed in tumors. NCAPG2, SMC2, and SMC4 are upregulated in various cancer types (Dávalos et al., 2012; De Keersmaecker et al., 2014; Murakami-Tonami et al., 2014; Zhan et al., 2017; Zhang et al., 2016; Zhou et al., 2014, 2012). Knockdown of these subunits causes decreased survival and proliferation of cancer cell lines (Dávalos et al., 2012; De Keersmaecker et al., 2014; Murakami-Tonami et al., 2014;

Zhan et al., 2017; Zhang et al., 2016; Zhou et al., 2014, 2012). These observations suggest that overexpression of condensin II subunits is associated with increased cancer cell survival. In this study, we determined that overexpression of WT CAPH2 caused only a relatively slight increase in anaphase defects in RPE1, and did not increase anaphase defects at all in HCT116 (Figure 3). Overexpression of WT CAPH2 did not increase CIN in either cell line tested (Figure 7), and while overexpression of WT CAPH2 did cause an increase in DNA damage foci in both cell lines tested, the damage foci were generated through a different kinase than with mutant CAPH2 (Figure 4g,h). Therefore, it is less likely that the overexpression of condensin II subunits observed in multiple tumor types (Zhan et al., 2017; Zhang et al., 2016; Zhou et al., 2014, 2012) is contributing to genomic instability in the same way as CAPH2 cancer-associated mutations. This study consequently furthers our understanding of the role of condensin II in cancer progression by revealing an important distinction between mutation of condensin II subunits, which we propose to be a source of genomic instability, and overexpression of WT condensin II subunits which supports increased proliferation (Dávalos et al., 2012; De Keersmaecker et al., 2014; Murakami-Tonami et al., 2014; Zhan et al., 2017; Zhang et al., 2016; Zhou et al., 2014, 2012).

ACKNOWLEDGMENTS

The authors would like to thank the Genomics and Molecular Biology Shared Resource and the Irradiation, Preclinical Imaging and Microscopy Resource at Dartmouth College. These core facilities were supported in part by a Cancer Center Core Grant (P30CA023108) from the National Cancer Institute. We were also supported by bioMT through NIH NIGMS grant P20-GM113132.

CONFLICT OF INTERESTS

The authors declare that there are no conflicts of interests.

AUTHOR CONTRIBUTIONS

Emily Weyburne and Giovanni Bosco conceived the study and designed experiments. Emily Weyburne conducted experiments and analyzed data. Emily Weyburne and Giovanni Bosco wrote the manuscript.

DATA AVAILABILITY STATEMENT

The data that support the findings of this study are available from the corresponding author upon reasonable request.

ORCID

Emily Weyburne http://orcid.org/0000-0001-7830-5259
Giovanni Bosco http://orcid.org/0000-0002-8889-9895

REFERENCES

Aalbers, A. M., Kajigaya, S., van den Heuvel-Eibrink, M. M., van der Velden, V. H. J., Calado, R. T., & Young, N. S. (2012). Human telomere disease due to disruption of the CCAAT box of the TERC promoter. *Blood*, *119*, 3060–3063.

d'Adda di Fagagna, Reaper, P. M., Clay-Farrace, L., Fiegler, H., Carr, P., Von Zglinicki, T., Saretzki, G., Carter, N. P., & Jackson, S. P. (2003). A DNA damage checkpoint response in telomere-initiated senescence. *Nature*, *426*, 194–198.

Baergen, A. K., Jeusset, L. M., Lichtensztejn, Z., & McManus, K. J. (2019). Diminished condensin gene expression drives chromosome instability that may contribute to colorectal cancer pathogenesis. *Cancers (Basel)*, *11*(8), 1066.

Bakhoum, S. F., & Landau, D. A. (2017). Chromosomal instability as a driver of tumor heterogeneity and evolution. *Cold Spring Harbor Perspectives in Medicine*, *7*, a029611.

Bakr, A., Oing, C., Kocher, S., Borgmann, K., Dornreiter, I., Petersen, C., Dikomey, E., & Mansour, W. Y. (2015). Involvement of ATM in homologous recombination after end resection and RAD51 nucleofilament formation. *Nucleic Acids Research*, *43*, 3154–3166.

Bauer, C. R., Hartl, T. A., & Bosco, G. (2012). Condensin II promotes the formation of chromosome territories by inducing axial compaction of polyploid interphase chromosomes. *PLoS Genetics*, *8*, e1002873.

Bodnar, A. G., Ouellette, M., Frolkis, M., Holt, S. E., Chiu, C. P., Morin, G. B., Harley, C. B., Shay, J. W., Lichtsteiner, S., & Wright, W. E. (1998). Extension of life-span by introduction of telomerase into normal human cells. *Science*, *279*, 349–352.

Burmann, F., Shin, H. C., Basquin, J., Soh, Y. M., Gimenez-Oya, V., Kim, Y. G., Oh, B. H., & Gruber, S. (2013). An asymmetric SMC-kleisin bridge in prokaryotic condensin. *Nature Structural & Molecular Biology*, *20*, 371–379.

Burrell, R. A., McGranahan, N., Bartek, J., & Swanton, C. (2013). The causes and consequences of genetic heterogeneity in cancer evolution. *Nature*, *501*, 338–345.

Burrell, R. A., McClelland, S. E., Endesfelder, D., Groth, P., Weller, M. C., Shaikh, N., Domingo, E., Kanu, N., Dewhurst, S. M., Gronroos, E., Chew, S. K., Rowan, A. J., Schenk, A., Sheffer, M., Howell, M., Kschischo, M., Behrens, A., Helleday, T., Bartek, J., … Swanton, C. (2013). Replication stress links structural and numerical cancer chromosomal instability. *Nature*, *494*, 492–496.

Capper, R., Britt-Compton, B., Tankimanova, M., Rowson, J., Letsolo, B., Man, S., Haughton, M., & Baird, D. M. (2007). The nature of telomere fusion and a definition of the critical telomere length in human cells. *Genes and Development*, *21*, 2495–2508.

Cesare, A. J., Kaul, Z., Cohen, S. B., Napier, C. E., Pickett, H. A., Neumann, A. A., & Reddel, R. R. (2009). Spontaneous occurrence of telomeric DNA damage response in the absence of chromosome fusions. *Nature Structural & Molecular Biology*, *16*, 1244–1251.

Cliby, W. A., Roberts, C. J., Cimprich, K. A., Stringer, C. M., Lamb, J. R., Schreiber, S. L., & Friend, S. H. (1998). Overexpression of a kinase-inactive ATR protein causes sensitivity to DNA-damaging agents and defects in cell cycle checkpoints. *EMBO Journal*, *17*, 159–169.

Coschi, C. H., Ishak, C. A., Gallo, D., Marshall, A., Talluri, S., Wang, J., Cecchini, M. J., Martens, A. L., Percy, V., Welch, I., Boutros, P. C., Brown, G. W., & Dick, F. A. (2014). Haploinsufficiency of an RB-E2F1-condensin II complex leads to aberrant replication and aneuploidy. *Cancer Discovery*, *4*, 840–853.

Crasta, K., Ganem, N. J., Dagher, R., Lantermann, A. B., Ivanova, E. V., Pan, Y., Nezi, L., Protopopov, A., Chowdhury, D., & Pellman, D. (2012). DNA breaks and chromosome pulverization from errors in mitosis. *Nature*, *482*, 53–58.

Cui, Y., Petrushenko, Z. M., & Rybenkov, V. V. (2008). MukB acts as a macromolecular clamp in DNA condensation. *Nature Structural & Molecular Biology*, *15*, 411–418.

Dávalos, V., Súarez-López, L., Castaño, J., Messent, A., Abasolo, I., Fernandez, Y., Guerra-Moreno, A., Espín, E., Armengol, M., Musulen, E., Ariza, A., Sayós, J., Arango, D., & Schwartz, S. (2012). Human SMC2 protein, a core subunit of human condensin complex, is a novel transcriptional target of the WNT signaling pathway and a

new therapeutic target. *Journal of Biological Chemistry*, *287*, 43472–43481.

De Keersmaecker, K., Porcu, M., Cox, L., Girardi, T., Vandepoel, R., de Beeck, J. O., Gielen, O., Mentens, N., Bennett, K. L., & Hantschel, O. (2014). NUP214-ABL1-mediated cell proliferation in T-cell acute lymphoblastic leukemia is dependent on the LCK kinase and various interacting proteins. *Haematologica*, *99*, 85–93.

Denchi, E. L., & de Lange, T. (2007). Protection of telomeres through independent control of ATM and ATR by TRF2 and POT1. *Nature*, *448*, 1068–1071.

Densham, R. M., Garvin, A. J., Stone, H. R., Strachan, J., Baldock, R. A., Daza-Martin, M., Fletcher, A., Blair-Reid, S., Beesley, J., Johal, B., Pearl, L. H., Neely, R., Keep, N. H., Watts, F. Z., & Morris, J. R. (2016). Human BRCA1-BARD1 ubiquitin ligase activity counteracts chromatin barriers to DNA resection. *Nature Structural & Molecular Biology*, *23*, 647–655.

Dowen, J. M., Bilodeau, S., Orlando, D. A., Hubner, M. R., Abraham, B. J., Spector, D. L., & Young, R. A. (2013). Multiple structural maintenance of chromosome complexes at transcriptional regulatory elements. *Stem Cell Reports*, *1*, 371–378.

Durkin, S. G., & Glover, T. W. (2007). Chromosome fragile sites. *Annual Review of Genetics*, *41*, 169–192.

Fenech, M., Kirsch-Volders, M., Natarajan, A. T., Surralles, J., Crott, J. W., Parry, J., Norppa, H., Eastmond, D. A., Tucker, J. D., & Thomas, P. (2011). Molecular mechanisms of micronucleus, nucleoplasmic bridge and nuclear bud formation in mammalian and human cells. *Mutagenesis*, *26*, 125–132.

Feng, L., Li, N., Li, Y., Wang, J., Gao, M., Wang, W., & Chen, J. (2015). Cell cycle-dependent inhibition of 53BP1 signaling by BRCA1. *Cell Discovery*, *1*, 15019.

Fouladi, B., Sabatier, L., Miller, D., Pottier, G., & Murnane, J. P. (2000). The relationship between spontaneous telomere loss and chromosome instability in a human tumor cell line. *Neoplasia*, *2*, 540–554.

Fouquin, A., Guirouilh-Barbat, J., Lopez, B., Hall, J., Amor-Gueret, M., & Pennaneach, V. (2017). PARP2 controls double-strand break repair pathway choice by limiting 53BP1 accumulation at DNA damage sites and promoting end-resection. *Nucleic Acids Research*, *45*, 12325–12339.

Fuentes-Perez, M. E., Gwynn, E. J., Dillingham, M. S., & Moreno-Herrero, F. (2012). Using DNA as a fiducial marker to study SMC complex interactions with the atomic force microscope. *Biophysical Journal*, *102*, 839–848.

George, C. M., Bozler, J., Nguyen, H. Q., & Bosco, G. (2014). Condensins are required for maintenance of nuclear architecture. *Cells*, *3*, 865–882.

Gibcus, J. H., Samejima, K., Goloborodko, A., Samejima, I., Naumova, N., Nuebler, J., Kanemaki, M. T., Xie, L., Paulson, J. R., Earnshaw, W. C., Mirny, L. A., & Dekker, J. (2018). A pathway for mitotic chromosome formation. *Science*, *359*, eaao6135.

Giunta, S., Belotserkovskaya, R., & Jackson, S. P. (2010). DNA damage signaling in response to double-strand breaks during mitosis. *Journal of Cell Biology*, *190*, 197–207.

Gosling, K. M., Makaroff, L. E., Theodoratos, A., Kim, Y. H., Whittle, B., Rui, L., Wu, H., Hong, N. A., Kennedy, G. C., Fritz, J. A., Yates, A. L., Goodnow, C. C., & Fahrer, A. M. (2007). A mutation in a chromosome condensin II subunit, kleisin beta, specifically disrupts T cell development. *Proceedings of the National Academy of Sciences of the United States of America*, *104*, 12445–12450.

Green, L. C., Kalitsis, P., Chang, T. M., Cipetic, M., Kim, J. H., Marshall, O., Turnbull, L., Whitchurch, C. B., Vagnarelli, P., Samejima, K., Earnshaw, W. C., Choo, K. H. A., & Hudson, D. F. (2012). Contrasting roles of condensin I and condensin II in mitotic chromosome formation. *Journal of Cell Science*, *125*, 1591–1604.

Hanahan, D., & Weinberg, R. A. (2011). Hallmarks of cancer: The next generation. *Cell*, *144*, 646–674.

Hartl, T. A., Sweeney, S. J., Knepler, P. J., & Bosco, G. (2008). Condensin II resolves chromosomal associations to enable anaphase I segregation in *Drosophila* male meiosis. *PLoS Genetics*, *4*, e1000228.

Hatch, E. M., Fischer, A. H., Deerinck, T. J., & Hetzer, M. W. (2013). Catastrophic nuclear envelope collapse in cancer cell micronuclei. *Cell*, *154*, 47–60.

Hirano, T. (2016). Condensin-based chromosome organization from bacteria to vertebrates. *Cell*, *164*, 847–857.

Hirota, T., Gerlich, D., Koch, B., Ellenberg, J., & Peters, J. M. (2004). Distinct functions of condensin I and II in mitotic chromosome assembly. *Journal of Cell Science*, *117*, 6435–6445.

Hockemeyer, D., Sfeir, A. J., Shay, J. W., Wright, W. E., & de Lange, T. (2005). POT1 protects telomeres from a transient DNA damage response and determines how human chromosomes end. *EMBO Journal*, *24*, 2667–2678.

Isono, M., Niimi, A., Oike, T., Hagiwara, Y., Sato, H., Sekine, R., Yoshida, Y., Isobe, S. Y., Obuse, C., Nishi, R., Petricci, E., Nakada, S., Nakano, T., & Shibata, A. (2017). BRCA1 directs the repair pathway to homologous recombination by promoting 53BP1 dephosphorylation. *Cell Reports*, *18*, 520–532.

Janssen, A., van der Burg, M., Szuhai, K., Kops, G. J., & Medema, R. H. (2011). Chromosome segregation errors as a cause of DNA damage and structural chromosome aberrations. *Science*, *333*, 1895–1898.

Kagami, Y., Ono, M., & Yoshida, K. (2017). Plk1 phosphorylation of CAP-H2 triggers chromosome condensation by condensin II at the early phase of mitosis. *Scientific Reports*, *7*, 5583.

Keenholtz, R. A., Dhanaraman, T., Palou, R., Yu, J., D'Amours, D., & Marko, J. F. (2017). Oligomerization and ATP stimulate condensin-mediated DNA compaction. *Scientific Reports*, *7*, 14279.

Kim, J. H., Lee, S. R., Li, L. H., Park, H. J., Park, J. H., Lee, K. Y., Kim, M. K., Shin, B. A., & Choi, S. Y. (2011). High cleavage efficiency of a 2A peptide derived from porcine teschovirus-1 in human cell lines, zebrafish and mice. *PLOS One*, *6*, e18556.

Kschonsak, M., Merkel, F., Bisht, S., Metz, J., Rybin, V., Hassler, M., & Haering, C. H. (2017). Structural basis for a safety-belt mechanism that anchors condensin to chromosomes. *Cell*, *171*, 588–600.

de Lange, T. (2018). Shelterin-mediated telomere protection. *Annual Review of Genetics*, *52*, 223–247.

Leiserson, M. D. M., Vandin, F., Wu, H. T., Dobson, J. R., Eldridge, J. V., Thomas, J. L., Papoutsaki, A., Kim, Y., Niu, B., McLellan, M., Lawrence, M. S., Gonzalez-Perez, A., Tamborero, D., Cheng, Y., Ryslik, G. A., Lopez-Bigas, N., Getz, G., Ding, L., & Raphael, B. J. (2015). Pan-cancer network analysis identifies combinations of rare somatic mutations across pathways and protein complexes. *Nature Genetics*, *47*, 106–114.

Lezaja, A., & Altmeyer, M. (2018). Inherited DNA lesions determine G1 duration in the next cell cycle. *Cell Cycle*, *17*, 24–32.

Lo, A. W., Sprung, C. N., Fouladi, B., Pedram, M., Sabatier, L., Ricoul, M., Reynolds, G. E., & Murnane, J. P. (2002). Chromosome instability as a result of double-strand breaks near telomeres in mouse embryonic stem cells. *Molecular and Cellular Biology*, *22*, 4836–4850.

Longworth, M. S., Herr, A., Ji, J. Y., & Dyson, N. J. (2008). RBF1 promotes chromatin condensation through a conserved interaction with the Condensin II protein dCAP-D3. *Genes and Development*, *22*, 1011–1024.

Manning, A. L., Longworth, M. S., & Dyson, N. J. (2010). Loss of pRB causes centromere dysfunction and chromosomal instability. *Genes and Development*, *24*, 1364–1376.

Marechal, A., & Zou, L. (2013). DNA damage sensing by the ATM and ATR kinases. *Cold Spring Harbor Perspectives in Biology*, *5*, a012716.

Martin, C. A., Murray, J. E., Carroll, P., Leitch, A., Mackenzie, K. J., Halachev, M., Fetit, A. E., Keith, C., Bicknell, L. S., Fluteau, A., Gautier, P., Hall, E. A., Joss, S., Soares, G., Silva, J., Bober, M. B., Duker, A., Wise, C. A., Quigley, A. J., … Jackson, A. P. (2016). Mutations in genes encoding condensin complex proteins cause

microcephaly through decatenation failure at mitosis. *Genes and Development*, *30*, 2158–2172.

Matoba, K., Yamazoe, M., Mayanagi, K., Morikawa, K., & Hiraga, S. (2005). Comparison of MukB homodimer versus MukBEF complex molecular architectures by electron microscopy reveals a higher-order multimerization. *Biochemical and Biophysical Research Communications*, *333*, 694–702.

McClintock, B. (1939). The behavior in successive nuclear divisions of a chromosome broken at meiosis. *Proceedings of the National Academy of Sciences of the United States of America*, *25*, 405–416.

McClintock, B. (1941). The stability of broken ends of chromosomes in *Zea mays*. *Genetics*, *26*, 234–282.

Moyzis, R. K., Buckingham, J. M., Cram, L. S., Dani, M., Deaven, L. L., Jones, M. D., Meyne, J., Ratliff, R. L., & Wu, J. R. (1988). A highly conserved repetitive DNA sequence, (TTAGGG)n, present at the telomeres of human chromosomes. *Proceedings of the National Academy of Sciences of the United States of America*, *85*, 6622–6626.

Murakami-Tonami, Y., Kishida, S., Takeuchi, I., Katou, Y., Maris, J. M., Ichikawa, H., Kondo, Y., Sekido, Y., Shirahige, K., Murakami, H., & Kadomatsu, K. (2014). Inactivation of SMC2 shows a synergistic lethal response in MYCN-amplified neuroblastoma cells. *Cell Cycle*, *13*, 1115–1131.

Onn, I., Aono, N., Hirano, M., & Hirano, T. (2007). Reconstitution and subunit geometry of human condensin complexes. *EMBO Journal*, *26*, 1024–1034.

Ono, T., Fang, Y., Spector, D. L., & Hirano, T. (2004). Spatial and temporal regulation of Condensins I and II in mitotic chromosome assembly in human cells. *Molecular Biology of the Cell*, *15*, 3296–3308.

Ono, T., Losada, A., Hirano, M., Myers, M. P., Neuwald, A. F., & Hirano, T. (2003). Differential contributions of condensin I and condensin II to mitotic chromosome architecture in vertebrate cells. *Cell*, *115*, 109–121.

Pei, J., Kim, B. H., & Grishin, N. V. (2008). PROMALS3D: A tool for multiple protein sequence and structure alignments. *Nucleic Acids Research*, *36*, 2295–2300.

Piazza, I., Rutkowska, A., Ori, A., Walczak, M., Metz, J., Pelechano, V., Beck, M., & Haering, C. H. (2014). Association of condensin with chromosomes depends on DNA binding by its HEAT-repeat subunits. *Nature Structural & Molecular Biology*, *21*, 560–568.

Rice, C., Shastrula, P. K., Kossenkov, A. V., Hills, R., Baird, D. M., Showe, L. C., Doukov, T., Janicki, S., & Skordalakes, E. (2017). Structural and functional analysis of the human POT1-TPP1 telomeric complex. *Nature Communications*, *8*, 14928.

Sabatier, L., Ricoul, M., Pottier, G., & Murnane, J. P. (2005). The loss of a single telomere can result in instability of multiple chromosomes in a human tumor cell line. *Molecular Cancer Research*, *3*, 139–150.

Samoshkin, A., Dulev, S., Loukinov, D., Rosenfeld, J. A., & Strunnikov, A. V. (2012). Condensin dysfunction in human cells induces nonrandom chromosomal breaks in anaphase, with distinct patterns for both unique and repeated genomic regions. *Chromosoma*, *121*, 191–199.

Sfeir, A., Kosiyatrakul, S. T., Hockemeyer, D., MacRae, S. L., Karlseder, J., Schildkraut, C. L., & de Lange, T. (2009). Mammalian telomeres resemble fragile sites and require TRF1 for efficient replication. *Cell*, *138*, 90–103.

Smogorzewska, A., Karlseder, J., Holtgreve-Grez, H., Jauch, A., & de Lange, T. (2002). DNA ligase IV-dependent NHEJ of deprotected mammalian telomeres in G1 and G2. *Current Biology*, *12*, 1635–1644.

Stiff, T., O'Driscoll, M., Rief, N., Iwabuchi, K., Lobrich, M., & Jeggo, P. A. (2004). ATM and DNA-PK function redundantly to phosphorylate H2AX after exposure to ionizing radiation. *Cancer Research*, *64*, 2390–2396.

Sutani, T., Sakata, T., Nakato, R., Masuda, K., Ishibashi, M., Yamashita, D., Suzuki, Y., Hirano, T., Bando, M., & Shirahige, K. (2015). Condensin targets and reduces unwound DNA structures associated with transcription in mitotic chromosome condensation. *Nature Communications*, *6*, 7815.

Takai, K. K., Kibe, T., Donigian, J. R., Frescas, D., & de Lange, T. (2011). Telomere protection by TPP1/POT1 requires tethering to TIN2. *Molecular Cell*, *44*, 647–659.

Takai, H., Smogorzewska, A., & de Lange, T. (2003). DNA damage foci at dysfunctional telomeres. *Current Biology*, *13*, 1549–1556.

Tervasmaki, A., Mantere, T., Eshraghi, L., Laurila, N., Tuppurainen, H., Ronkainen, V. P., Koivuluoma, S., Devarajan, R., Peltoketo, H., & Pylkas, K. (2019). Tumor suppressor MCPH1 regulates gene expression profiles related to malignant conversion and chromosomal assembly. *International Journal of Cancer*, *145*, 2070–2081.

Thompson, S. L., & Compton, D. A. (2008). Examining the link between chromosomal instability and aneuploidy in human cells. *Journal of Cell Biology*, *180*, 665–672.

Tijhuis, A. E., Johnson, S. C., & McClelland, S. E. (2019). The emerging links between chromosomal instability (CIN), metastasis, inflammation and tumour immunity. *Molecular Cytogenetics*, *12*, 17.

Trimborn, M., Schindler, D., Neitzel, H., & Hirano, T. (2006). Misregulated chromosome condensation in MCPH1 primary microcephaly is mediated by condensin II. *Cell Cycle*, *5*, 322–326.

Tubbs, A., & Nussenzweig, A. (2017). Endogenous DNA damage as a source of genomic instability in cancer. *Cell*, *168*, 644–656.

Umbreit, N. T., Zhang, C. Z., Lynch, L. D., Blaine, L. J., Cheng, A. M., Tourdot, R., Sun, L., Almubarak, H. F., Judge, K., Mitchell, T. J., Spektor, A., & Pellman, D. (2020). Mechanisms generating cancer genome complexity from a single cell division error. *Science*, *368*(6488), eaba0712.

Uziel, T., Lerenthal, Y., Moyal, L., Andegeko, Y., Mittelman, L., & Shiloh, Y. (2003). Requirement of the MRN complex for ATM activation by DNA damage. *EMBO Journal*, *22*, 5612–5621.

Vannier, J. B., Pavicic-Kaltenbrunner, V., Petalcorin, M. I., Ding, H., & Boulton, S. J. (2012). RTEL1 dismantles T loops and counteracts telomeric G4-DNA to maintain telomere integrity. *Cell*, *149*, 795–806.

Venkatesh, T., Nagashri, M. N., Swamy, S. S., Mohiyuddin, S. M., Gopinath, K. S., & Kumar, A. (2013). Primary microcephaly gene MCPH1 shows signatures of tumor suppressors and is regulated by miR-27a in oral squamous cell carcinoma. *PLOS One*, *8*, e54643.

Wallace, H. A., Rana, V., Nguyen, H. Q., & Bosco, G. (2019). Condensin II subunit NCAPH2 associates with shelterin protein TRF1 and is required for telomere stability. *Journal of Cellular Physiology*, *234*, 20755–20768.

Wang, N., Lu, H., Chen, W., Gan, M., Cao, X., Zhang, J., & Chen, L. (2014). Primary microcephaly gene MCPH1 shows a novel molecular biomarker of human renal carcinoma and is regulated by miR-27a. *International Journal of Clinical and Experimental Pathology*, *7*, 4895–4903.

Weber, A. M., & Ryan, A. J. (2015). ATM and ATR as therapeutic targets in cancer. *Pharmacology and Therapeutics*, *149*, 124–138.

Woo, J. S., Lim, J. H., Shin, H. C., Suh, M. K., Ku, B., Lee, K. H., Joo, K., Robinson, H., Lee, J., Park, S. Y., Ha, N. C., & Oh, B. H. (2009). Structural studies of a bacterial condensin complex reveal ATP-dependent disruption of intersubunit interactions. *Cell*, *136*, 85–96.

Woodward, J., Taylor, G. C., Soares, D. C., Boyle, S., Sie, D., Read, D., Chathoth, K., Vukovic, M., Tarrats, N., Jamieson, D., Campbell, K. J., Blyth, K., Acosta, J. C., Ylstra, B., Arends, M. J., Kranc, K. R., Jackson, A. P., Bickmore, W. A., & Wood, A. J. (2016). Condensin II mutation causes T-cell lymphoma through tissue-specific genome instability. *Genes and Development*, *30*, 2173–2186.

Yamashita, D., Shintomi, K., Ono, T., Gavvovidis, I., Schindler, D., Neitzel, H., Trimborn, M., & Hirano, T. (2011). MCPH1 regulates chromosome condensation and shaping as a composite modulator of condensin II. *Journal of Cell Biology*, *194*, 841–854.

Zawadzka, K., Zawadzki, P., Baker, R., Rajasekar, K. V., Wagner, F., Sherratt, D. J., & Arciszewska, L. K. (2018). MukB ATPases are

regulated independently by the N- and C-terminal domains of MukF kleisin. *eLife*, *7*, e31522.

Zhan, P., Xi, G., Zhang, B., Wu, Y., Liu, H., Liu, Y., Xu, W., Zhu, Q., Cai, F., Zhou, Z., Miu, Y., Wang, X., Jin, J., Li, Q., Lv, T., & Song, Y. (2017). NCAPG2 promotes tumour proliferation by regulating G2/M phase and associates with poor prognosis in lung adenocarcinoma. *Journal of Cellular and Molecular Medicine*, *21*, 665–676.

Zhang, C., Kuang, M., Li, M., Feng, L., Zhang, K., & Cheng, S. (2016). SMC4, which is essentially involved in lung development, is associated with lung adenocarcinoma progression. *Scientific Reports*, *6*, 34508.

Zhang, C. Z., Leibowitz, M. L., & Pellman, D. (2013). Chromothripsis and beyond: Rapid genome evolution from complex chromosomal rearrangements. *Genes and Development*, *27*, 2513–2530.

Zhang, C. Z., Spektor, A., Cornils, H., Francis, J. M., Jackson, E. K., Liu, S., Meyerson, M., & Pellman, D. (2015). Chromothripsis from DNA damage in micronuclei. *Nature*, *522*, 179–184.

Zhou, B., Chen, H., Wei, D., Kuang, Y., Zhao, X., Li, G., Xie, J., & Chen, P. (2014). A novel miR-219-SMC4-JAK2/Stat3 regulatory pathway in human hepatocellular carcinoma. *Journal of Experimental & Clinical Cancer Research*, *33*, 55.

Zhou, B., Yuan, T., Liu, M., Liu, H., Xie, J., Shen, Y., & Chen, P. (2012). Overexpression of the structural maintenance of chromosome 4 protein is associated with tumor de-differentiation, advanced stage and vascular invasion of primary liver cancer. *Oncology Reports*, *28*, 1263–1268.

Zimmermann, M., & de Lange, T. (2014). 53BP1: Pro choice in DNA repair. *Trends in Cell Biology*, *24*, 108–117.

SUPPORTING INFORMATION

Additional Supporting Information may be found online in the supporting information tab for this article.

How to cite this article: Weyburne E, Bosco G. Cancer-associated mutations in the condensin II subunit CAPH2 cause genomic instability through telomere dysfunction and anaphase chromosome bridges. *J Cell Physiol*. 2021;236: 3579–3598. https://doi.org/10.1002/jcp.30113